ATMOSPHERIC ENVIRONMENT: X 13 (2022) 100159

Contents lists available at ScienceDirect

Atmospheric Environment: X

journal homepage: www.journals.elsevier.com/atmospheric-environment-x

Chemical composition and sources of organic aerosol on the Adriatic coast in Croatia

R. Casotto [a], A. Cvitešić Kušan [b], D. Bhattu [a,1], T. Cui [a], M.I. Manousakas [a], S. Frka [b], A. Kroflič [c], I. Grgić [c], I. Ciglenečki [d], U. Baltensperger [a], J.G. Slowik [a], K.R. Daellenbach [a,**], A.S.H. Prévôt [a,*]

[a] Laboratory of Atmospheric Chemistry, Paul Scherrer Institute, CH-5232, Villigen-PSI, Switzerland
[b] Laboratory for Marine and Atmospheric Biogeochemistry, Division for Marine and Environmental Research, Ruđer Bošković Institute, 10000, Zagreb, Croatia
[c] Department of Analytical Chemistry, National Institute of Chemistry, 1000, Ljubljana, Slovenia
[d] Laboratory for Physical Oceanography and Chemistry of Aquatic Systems, Division for Marine and Environmental Research, Ruđer Bošković Institute, 10000, Zagreb, Croatia

ARTICLE INFO

Keywords:
Organic aerosol
Secondary aerosol
Source apportionment
Chemical characterization
Adriatic sea
Coast
Croatia
HR-ToF-AMS
EESI-TOF
SOOA
BBOA

ABSTRACT

Air pollution studies are still scarce in some areas in Europe like around the Adriatic Sea. Source apportionment of the fine particulate ($PM_{2.5}$) organic aerosol (OA) was conducted near Rogoznica, a small touristic settlement on the Eastern Adriatic coast of Croatia, near Lake Rogoznica (43.53° N, 15.95° E). Filter-based offline analyses of PM by a high resolution time-of-flight aerosol mass spectrometer (HR-ToF-AMS) and an extractive electrospray ionization time-of-flight mass spectrometer (EESI-TOF) were used to apportion OA to its sources. We quantified the contributions of fresh biomass burning OA (BBOA) and three oxygenated OA (OOA), denoted as background OOA (bkgOOA), summer OOA (SOOA), and sulfur-containing OOA (SC-OOA). The bkgOOA component correlates with anthropogenically influenced secondary inorganic aerosol constituents (e.g. sulfate) and dominates OA both during the warm and cold seasons (44%). It exhibits characteristics of regional SOA and there are indications that during the warm season SOA from wildfires could be a substantial contributor. EESI-TOF measurements of the levoglucosan related ion showed a high correlation with the BBOA factor. Secondary OA has a similar molecular composition during the cold and warm seasons – in line with the large contribution of bkgOOA throughout the investigated seasons. SOOA comprises 19% of total OA and increases exponentially with the local temperature, consistent with SOA production by oxidation of biogenic emissions. In addition to biogenic precursors, other precursors (alkanes and aromatic) may contribute to the OOA enhancement during the warm season. SC-OOA is a minor contributor to OA (6%) and is most likely linked to emissions from a close-by marine lake.

1. Introduction

Atmospheric aerosols strongly affect human health and Earth's climate, causing an estimated 3.3 million annual premature deaths worldwide and comprising the largest source of uncertainty in global radiative forcing estimates (Burnett et al., 2018; IPCC, 2021; WHO, 2018). It is generally accepted that any increase in total particulate matter (PM) is going to increase mortality rates, but different sources will contribute to this increase in different amounts. Total PM has been linked to health problems by epidemiological studies (Dockery et al., 1992, 1993), and more recent work indicates that aerosol health effects could strongly depend on the composition of PM, of which organic aerosol (OA), especially secondary organic aerosol (SOA), is an important constituent (Daellenbach et al., 2020). Up to 90% of the share of the atmospheric fine suspended particulate matter (particulate matter with an aerodynamic diameter smaller than 1 μm, PM_1) is OA (Jimenez et al., 2009). Because OA composition and concentration are governed by source emissions and subsequent atmospheric processing, OA source apportionment is of high importance in developing air quality standards and in policy making. In the past two decades, new instrumentation,

* Corresponding author.
** Corresponding author.
E-mail addresses: kaspar.daellenbach@psi.ch (K.R. Daellenbach), andre.prevot@psi.ch (A.S.H. Prévôt).
[1] now at Department of Civil and Infrastructure Engineering, Indian Institute of Technology Jodhpur, Jodhpur, 342 037, India.

https://doi.org/10.1016/j.aeaoa.2022.100159
Received 27 October 2021; Received in revised form 8 February 2022; Accepted 11 February 2022
Available online 14 February 2022

such as the aerosol mass spectrometer (AMS) and the extractive electrospray ionization time-of-flight mass spectrometer (EESI-TOF, applying a soft ionization method), have allowed a deeper insight in the chemical composition of aerosol PM. Source apportionment analyses relying on positive matrix factorization (PMF) have greatly improved the identification of the sources of OA. PMF is a bilinear receptor model that is able to separate complex sets of data into positive sources concentration time series and their corresponding constant chemical composition. When applied to OA mass spectra, PMF is typically able to separate the OA mix into primary (POA) sources characterized by low oxidation levels, e.g., hydrocarbon-like OA (HOA) or biomass burning OA (BBOA), and SOA types characterized by higher oxidation levels due to their longer presence in the atmospheric oxidative environment. PMF was first applied to offline marker data (Jaeckels et al., 2007), and later used for online OA mass spectral data (Lanz et al., 2007), and finally applied to offline OA mass spectra (Bozzetti et al., 2016, 2017a, 2017b; Daellenbach et al., 2017, 2020; Qi et al., 2020; Srivastava et al., 2021; Vlachou et al., 2018, 2019). The offline method consists in the measurements of filter extracts after filter sample collection in the field.

Eastern Adriatic coastal sites are known to be influenced by long-range transport of continental emissions from the highly polluted Southeastern Europe region (De Pieri et al., 2014; Huremović et al., 2020; Kanakidou et al., 2011; Pehnec et al., 2020; Škarek et al., 2007; Stanic et al., 2012; Talić et al., 2018; Turšič et al., 2006), as well as by local sources such as ship emissions (Merico et al., 2016), and open-fire episodes typical of the Mediterranean coastal area (Cvitešić Kušan et al., 2020). Airborne aerosol mass spectrometer measurements over the northern Adriatic Sea (Crosier et al., 2007; Highwood et al., 2007) showed that much of the aerosol is secondary, with nitrate and ammonia predominantly coming from the large sources in the Po Valley, and sulfate (mostly as ammonium sulfate) and organic aerosol from the air masses from the east. With the exception of the Northern part (e.g. Gregoris et al. (2021); Mifka et al. (2021)), to our knowledge, no detailed source apportionment of the OA fraction has been conducted for locations at the Eastern Adriatic coastal area. We need to emphasize that the Mediterranean region is one of the most susceptible areas to climate change (Chenoweth et al., 2011; García-Ruiz et al., 2011; Giorgi and Lionello, 2008; Lelieveld et al., 2002, 2012; Sanchez-Gomez et al., 2009) and therefore providing anchors to fine scale climate models is of great importance, as well as increasing the number of sampling sites to improve the spatial resolution of the measurements.

Thus, this work is focused on identifying and quantifying the OA sources at a coastal Adriatic location in Croatia. We make use of a recently developed framework for off-line analysis of PM collected on filter samples (Daellenbach et al., 2016). Chemical characterization of the organic aerosol is obtained by the high resolution time-of-flight aerosol mass spectrometer (HR-ToF-AMS) (DeCarlo et al., 2006), supported by EESI-TOF (Lopez-Hilfiker et al., 2019; Qi et al., 2019; Stefenelli et al., 2019). Chemical composition data on the same filter set already performed previously (Cvitešić Kušan et al., 2020) were also used in support of source apportionment analysis by PMF.

2. Methods

2.1. Study location

The study site was on the shore of the marine lake Rogoznica, also known as Dragon's Eye lake, located on the Gradina Peninsula near the small touristic settlement of Rogoznica (43°31′52"N 15°57′34"E, around 1600 inhabitants), about 30 km south of Šibenik (34 000 inhabitants) and 40 km west of Split (178 000 inhabitants) on the middle Adriatic coast in Croatia, and in the area of the yacht club Marina Frapa. This central Adriatic marine region is taken as a relatively clean area (Cvitešić Kušan et al., 2020), with measured values of airborne $PM_{2.5}$ up to 10–12 μg/m^3 on average. The location is characterized by fields in the karst landscape and Mediterranean vegetation, with tourism and mariculture activities. Mountains are located to the north and northeast. Summers are arid, as is typical for the Mediterranean region, and thus prone to wildfires. The Rogoznica lake is enriched with sulfur compounds. During water stratification, low concentrations of organosulfur compounds are present in the surface oxic layer (up to 20 nM), while sulfide is accumulating in the anoxic bottom layer. During lake mixing sulfide from the anoxic layer reaches the surface where it is rapidly partly oxidized (mainly to S^0) and some part is further lost into the atmosphere. The effect of this process is already recorded by the presence of sulfide-like compounds in PM collected in autumn of 2016 (Cvitešić Kušan et al., 2019).

2.2. Particulate matter filter collection

$PM_{2.5}$ was collected seasonally between 8 April 2015 and 5 December 2016 by a low volume sequential sampler (SEQ47/50, Sven Leckel, Ingenieurbüro GmbH, Germany) using pre-combusted (at 450 °C for 4 h) glass-fiber filters (Whatman, Grade GF/F, d = 47 mm). The sampler utilized a flow rate of 2.3 m^3/h over a 48 h collection period for each filter. Filter samples were placed in Petri slides and stored at −20 °C. Field blank (FB) filters were processed the same way as the collected samples. A total of 168 filters were processed for measurements, as well as 8 FB filters. Because of EESI-TOF instability and the corruption of one raw data file, a total of 147 filters and 6 FB filters were measured by both HR-ToF-AMS and EESI-TOF.

2.3. Chemical analyses and instrumentation

The off-line measurement and analysis procedure was based on the analytical framework developed for the HR-ToF-AMS by Daellenbach et al. (2016) and adapted for the EESI-TOF by Qi et al. (2020), and only a brief description is provided here. A punch of filter area 3.14 cm^2 was submerged in 10 mL of ultra-pure water (Milli-Q®, 18.2 MΩ cm at 25 °C, total organic carbon, TOC <5 ppb, Merck), sonicated at 30 °C for 20 min and then vortexed for 60 s. The extract was filtered through a nylon membrane with 0.22 μm pores (Infochroma AG, Yeti HPLC filters, 13 mm diameter) in order to remove the residual material of the filter and larger insoluble particles to avoid clogging the nebulizer or mass spectrometer inlets during measurements. Each sample was spiked with 0.1 mL of 200 ppm solutions of isotopically-labelled ammonium sulfate $(NH_4)_2{}^{34}SO_4$ and ammonium nitrate $NH_4{}^{15}NO_3$ to ensure a particle size that was efficiently transmitted through the AMS' aerodynamic lens, independent of the concentration in the extract, and to monitor the HR-ToF-AMS performance. In addition, the ratio of OA/$^{15}NO_3$ was used to estimate the water soluble organic aerosol (WSOA) concentration corresponding to the HR-ToF-AMS measurements (see section 2.4) for 6 filters and 6 FB filters missing WSOC measurements. The labelled ammonium sulfate was not used for data analysis. These samples were then nebulized using argon gas (99.999% purity) and passed through an APEX Q nebulizer (Elemental Scientific Inc.) (Bozzetti et al., 2016; Daellenbach et al., 2016; Qi et al., 2020). Each filter extract was nebulized for 480 s, and preceded by a measurement of ultra-pure water (blank) for 720 s to which it is associated. The flux of argon (1.2 L/min) containing the nebulized sample was bifurcated, part of it (0.1 L/min) going to the AMS, and most of the remaining (1 L/min) to the EESI-TOF inlet. Excess flow was discarded just before entering the EESI-TOF. A Nafion™ dryer (Perma Pure™) was placed in front of the bifurcation to maintain the relative humidity in the sampled flow below ~40%, which reduces aerosol water content and protects the instruments from excessive water inflow.

The HR-ToF-AMS focuses the nebulized and dried particles through an aerodynamic lens and introduces the resulting particle beam into a high vacuum chamber. Once inside, the particles impact on a surface heated to 600 °C (10^{-7} torr) to vaporize all non-refractory constituents. The resulting gaseous molecules are ionized by electron ionization (70 eV). This provides quantitative aerosol mass spectra but also extensive

thermal decomposition and ionization-induced fragmentation, leading to a substantial loss in chemical information. Small packets of ions, triggered by an intermittent starter electric field, enter the time-of-flight mass spectrometer. An in-depth description of the operating principles of the HR-ToF-AMS can be found in Canagaratna et al. (2007). One recorded spectrum represents a 36.5 s average.

The EESI-TOF consists of an extractive electrospray ionization (EESI) inlet coupled to a time-of-flight mass spectrometer, and has been described in detail elsewhere (Lopez-Hilfiker et al., 2019). The aerosol is first passed through a denuder to eliminate the gaseous fraction. The EESI inlet intersects the aerosol particles with a charged spray of 1:1 water:acetonitrile (ACN) (HPLC grade, ≥99.9% purity, Sigma-Aldrich, St. Louis, USA), doped with 100 ppm of sodium iodide (NaI), resulting in extraction and ionization of the detectable fraction (i.e., soluble and ionizable compounds). Sodium iodide suppresses unwanted ionization pathways and simplifies spectral interpretation by ensuring ions are predominantly detected as $[M]Na^+$ (7% of the ions are still detected as $[M]H^+$, making up an average of 17.8% of the total raw signal). The droplets enter the vacuum region through a heated inlet (~270 °C). Because the residence time is very short (a few μs), the effective temperature experienced by the droplets is much lower than the inlet temperature, and no thermal decomposition is observed. The combination of gentle heating and vacuum causes water evaporation from the droplets, leading to ejection of unfragmented molecular ions, mainly as clusters with Na^+. These cluster ions are detected by a time-of-flight mass spectrometer operating in positive ion mode. One recorded spectrum represents a 32.5 s average.

Additional measurements performed on the filters include the following. $PM_{2.5}$ mass was measured with a Mettler Toledo XP205DR microbalance. The filters were weighed before and after sampling at the same temperature (20 ± 1 °C) and relative humidity (50 ± 5%). Ion chromatography analyses were performed with a Dionex ICS 3000 equipped with a conductivity detector. A precolumn (Dionex IonPac AG11-HC, 4 × 50 mm) and an analytical column (Dionex IonPac AS11-HC, 4 × 250 mm) were used to separate and quantify 12 anions in the following order: fluoride (F^-), lactate ($C_3H_5O_3^-$), acetate ($C_2H_3O^{2-}$), formate (CHO_2^-), methanesulfonate ($CH_3SO_3^-$, MS^-), chloride (Cl^-), nitrate (NO_3^-), malate ($C_4H_4O_5^{2-}$), maleate ($C_4H_2O_4^{2-}$), sulfate (SO_4^{2-}), oxalate ($C_2O_4^{2-}$), and phosphate (PO_4^{3-}). The cations sodium (Na^+), ammonium (NH_4^+), and potassium (K^+) were measured on a Thermo Separation Products ion chromatograph equipped with a Shodex CD-5 conductivity detector, using a Dionex IonPac CG/CS12A precolumn (4 × 50 mm) and column (4 × 250 mm). Analyses of water-soluble ions were performed previously on each filter sample and details can be found in Cvitešić Kušan et al. (2020). Water soluble organic carbon (WSOC, extracts prepared analogously to the ones used for offline AMS analyses – 2.4) was determined by high-temperature catalytic oxidation (HTCO) method by a TOC-V_{CPH} analyzer with a non-dispersive infrared (NDIR) detector for CO_2 (Shimadzu, Japan), and total organic carbon (OC) was analyzed with a solid sample module (SSM-5000A) associated with a TOC-V_{CHP} analyzer. These measurements were used in support of the OA source apportionment analysis conducted in this study.

2.4. Offline AMS analysis

The analysis of the AMS dataset is based on the method developed by Daellenbach et al. (2016). Data analysis started with raw AMS data processed through SQUIRREL (SeQUential Igor data RetRiEvaL v. 1.63; D. Sueper, University of Colorado, Boulder, CO, USA) and PIKA (Peak Integration and Key Analysis v. 1.23) to obtain mass spectra of identified ions over the m/z range 12–120. The PIKA software outputs the raw data matrix $\mathbf{M}^{raw}$ with elements $m_{i,j}^{raw}$, and the single-ion error time series δ_i which accounts for electronic noise and ion-to-ion variability at the detector, where i is the instrument time index and j the ion index. 309 organic ions were detected and exported by PIKA. $\mathbf{M}^{raw}$ and δ_i were used to calculate the final offline data matrix $\mathbf{M}^{offline}$ with elements $m_{\alpha,j}^{offline}$, and the corresponding error matrix $\mathbf{E}^{offline}$ composed of elements $\sigma_{\alpha,j}^{offline}$. The index α runs over the $N_{Filters} = 153$ filters considered, among which are the 6 field blanks (FB). To each filter α corresponds a number N_{Filter_α} of mass spectra of filter-sample (denoted with indices $i\varepsilon Filter_\alpha$) and a number N_{Blank_α} of preceding water-blank measurements (denoted with indices $i\varepsilon Blank_\alpha$). The WSOA spectra of the collected particles, i.e., the rows of matrix $\mathbf{M}^{offline}$, were determined as

$$m_{\alpha,j}^{offline} = S_{\alpha,j}^{Filter_\alpha} - S_{\alpha,j}^{Blank_\alpha} = \frac{\sum_{i\in Filter_\alpha} m_{i,j}^{raw}}{N_{Filter_\alpha}} - \frac{\sum_{i\in Blank_\alpha} m_{i,j}^{raw}}{N_{Blank_\alpha}}, \quad (1)$$

where each $S_{\alpha,j}$ corresponds to the average of elements $m_{i,j}^{raw}$ over the corresponding subset of measurements. The error associated with each ion signal was determined by first calculating the standard deviation of the previously obtained averages, namely

$$\sigma_{\alpha,j}^{filter} = \sqrt{\frac{\sum_{i\in Filter_\alpha}\left(m_{i,j}^{raw} - S_{\alpha,j}^{Filter_\alpha}\right)^2}{N_{Filter_\alpha} - 1}} \quad (2)$$

for the filter, and

$$\sigma_{\alpha,j}^{blank} = \sqrt{\frac{\sum_{i\in Blank_\alpha}\left(m_{i,j}^{raw} - S_{\alpha,j}^{Blank_\alpha}\right)^2}{N_{Blank_\alpha} - 1}} \quad (3)$$

for the blank. Whenever the error was smaller than the minimum error $\delta_{\alpha,j}$ accounting for the duty cycle correction, the minimum error was used as error. The total error associated to filter related ions is thus obtained as

$$e_{\alpha,j}^{filter} = \max\left(\delta_{\alpha,j}^{filter},\ \sigma_{\alpha,j}^{filter}\right). \quad (6)$$

Similarly, the total error associated to blank-related ions is expressed as

$$e_{\alpha,j}^{blank} = \max\left(\delta_{\alpha,j}^{blank},\ \sigma_{\alpha,j}^{blank}\right). \quad (7)$$

The error associated to $m_{\alpha,j}^{final}$ is thus calculated as

$$\sigma_{\alpha,j}^{offline} = \sqrt{\left(e_{\alpha,j}^{filter}\right)^2 + \left(e_{\alpha,j}^{blank}\right)^2}. \quad (8)$$

The mean signal to noise ratio of each ion SNR_j was calculated as

$$SNR_j = \frac{\sum_\alpha\left(m_{\alpha,j}^{offline} / \sigma_{\alpha,j}^{offline}\right)}{N_{Filters}}. \quad (9)$$

All ions with $SNR_j < 0.2$ were not considered, leaving 206 ions in $\mathbf{M}^{offline}$. The error $\sigma_{\alpha,j}^{offline}$ is linearly increased for ions with $0.2 < SNR_j < 2$, starting from a scaling factor of 1 at $SNR_j = 2$ to a scaling factor of 10 at $SNR_j = 0.2$.

The CO_2^+ peak and the related peaks of CO^+, H_2O^+, HO^+, and O^+ were corrected using pure ammonium nitrate measurements by adapting the AMS fragmentation table as proposed by Pieber et al. (2016) and Daellenbach et al. (2017). Equation (10) was used to correct the measured CO_2^+ to the real estimate.

$$CO_{2,real} = CO_{2,meas} - \left(\frac{CO_{2,meas}}{NO_{3,\ meas}}\right)_{NH_4NO_{3,pure}} \cdot NO_{3,meas} \quad (10)$$

Because H_2O^+, HO^+, and O^+ are not directly measured but rather calculated as a constant fraction of CO_2^+ signal, the uncertainties of all four ions were increased by a factor 2 (i.e. $\sqrt{4}$), to avoid overweighting the CO_2^+ time series. Note that unlike for PMF analyses of online AMS data, it is not necessary to include CO^+ in this correction, as the use of Ar as a carrier gas circumvents the interference with N_2^+ that prevents direct measurement of CO^+ in a conventional operation mode (Bozzetti

et al., 2017b). The organic AMS spectra were then scaled to WSOA using the WSOC measurement and the organic aerosol to organic carbon ratio (OA/OC) calculated from each spectrum using the Igor analysis kit APES (Analytical Procedure for Elemental Separation, Aiken et al. (2008), for consistency using the fragmentation table for H_2O^+, HO^+, O^+, CO^+).

Assuming that $^{15}NO_3$ and NO_3 have the same ionization efficiency, the estimated nitrate concentration in the air during sampling can be expressed as

$$NO_{3,estimate} = \frac{NO_{3,AMS}}{^{15}NO_{3,AMS}} mass(^{15}NO_3) \frac{A_F}{A_p} \frac{1}{V}, \quad (11)$$

where $mass(^{15}NO_3)$ is the mass of labelled nitrate added to each sample before the analysis, $NO_{3,AMS}$ *is the sum of the AMS-detected frequencies of* NO_3 related ions (N^+, NO^+, NO_2^+), $^{15}NO_{3,AMS}$ *is the sum of the AMS-detected frequencies of* $^{15}NO_3$ related ions ($^{15}N^+$, $^{15}NO^+$, $^{15}NO_2^+$), A_F is the area of the filter that collected the aerosol, A_p is the punched area of the filter used for the measurement, and V is the volume of air passed through the filter during collection. $NO_{3,AMS}$ and $^{15}NO_{3,AMS}$ were calculated summing up the mentioned ions. No NO_3^+ or $^{15}NO_3^+$ was used as their detected signals were negligible. Fig. S1 shows the result of the calculations compared with measured nitrate concentrations by ion chromatography in a log-log reference frame for a better view of all the points ranging over multiple orders of magnitude, but mainly concentrated in the lower left side of the plot. The slope of the linear fit is 1.05 ± 0.04, very close to 1 as expected.

Assuming an AMS-measured quantity M is quantitatively collected by the filters (e.g., M does not volatilize or react on the filter surface) and is fully extracted, M can be estimated by substituting $NO_{3,AMS}$ with M/RIE_M in Equation (11), where RIE_M is the relative ionization efficiency of species M with respect to the nitrate. This method was used to estimate the WSOC concentrations for the 6 FB filters and 6 filters that were not successfully analyzed by the TOC analyzer. Thus, the sum of all the AMS-measured OA species Org_S was used to find the WSOC estimate through the formula

$$WSOC_{estimate} = \frac{Org_S}{RIE_{OA}\left(OA/OC\right)} \frac{1}{^{15}NO_{3,AMS}} mass(^{15}NO_3) \frac{A_F}{A_p} \frac{1}{V}, \quad (12)$$

where RIE_{OA} is assumed to be 1.4 (Canagaratna et al., 2007). In order to confirm the validity of the procedure, $WSOC_{estimate}$ values were calculated for all filters. Fig. 1 shows the scatter plot between WSOC concentrations determined through this procedure and the measurements of WSOC from the TOC analyzer, as well as the related linear fit. The AMS-WSOC estimate is lower than the concentrations determined by the TOC analyzer (fit slope of 0.85 ± 0.05, 3σ deviation from the expected result of 1). The estimated WSOC missing values were thus scaled with the inverse of the linear fit to correct for the bias. The final WSOA spectra was obtained by scaling the spectra to WSOA (product of WSOC and OA/OC) and then subtracting from each filter spectrum the average spectrum of the WSOA field blank filters (and the resulting uncertainty propagated to the error matrix used for PMF input).

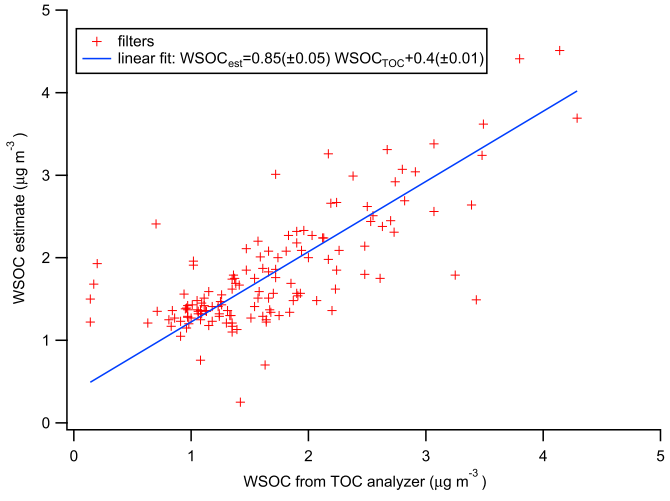

Fig. 1. Scatter plot of the WSOC concentrations estimated based on the AMS analyses using $^{15}NO_3$ as an internal standard and the WSOC concentrations measured by a TOC analyzer.

2.5. Offline EESI-TOF analysis

EESI-TOF raw data were first processed using the software Tofware (TOFWERK AG) to obtain the integrated matrix $\mathbf{I}^{raw}$ of signal spectra (974 ions fitted over the m/z range 110–400) with a time resolution of 32.5 s, with elements $I_{i,j}^{raw}$, and minimum error time series $^{EESI-TOF}\delta_i$. The process to obtain the final data matrix $\mathbf{I}^{offline}$ (with elements $I_{\alpha,j}^{offline}$), as well as the corresponding error matrix $\mathbf{E}^{\mathbf{I},offline}$ (with elements $\sigma_{\alpha,j}^{\mathbf{I},offline}$), follows the same procedure used for the AMS measurements in Section 2.3 (Equation (1) through Equation (8)).

Unlike the AMS, the EESI-TOF spectra were not normalized before scaling by WSOC. This is because normalization assumes that the total measured mass is proportional to the real concentration of the aerosol in the atmosphere; that is, all measured ions are detected with the same sensitivity. Such an assumption is not valid for the EESI-TOF, because the effective sensitivity of the EESI-TOF depends on the molecular identity and no generally applicable parameterization exists (Lopez-Hilfiker et al., 2019; Wang et al., 2021). Thus, the calculation to obtain the specific mass flux (SMF) to the EESI-TOF detector was carried out as

$$SMF_{\alpha,j} = \frac{I_{\alpha,j}^{offline} \cdot WSOC_\alpha \cdot {}^{AMS}\left(\frac{OA}{OC}\right)_\alpha \cdot MW_j}{average_\alpha\left(WSOC_\alpha \cdot {}^{AMS}\left(\frac{OA}{OC}\right)_\alpha\right)} \quad (13)$$

where $^{AMS}(OA/OC)_\alpha$ is the organic aerosol to organic carbon ratio of filter α as found in the AMS measurements, MW_j is the mass weight of ion j (excluding the weight of Na^+ or H^+ in case of such clusters), and $WSOC_\alpha$ the water soluble organic carbon of filter α. The errors $\sigma_{\alpha,j}^{offline}$ were scaled with the same scaling factors to obtain $\sigma_{\alpha,j}^{SMF}$. The spectra of the four (blank-subtracted) field blank filters were then averaged and subtracted from each filter spectrum and the error propagated, obtaining the final matrices with elements $SMF_{\alpha,j}^{final}$ and $\sigma_{\alpha,j}^{SMF,final}$.

Subsequently, the mass spectral matrix was cleaned by considering the signal to noise ratio calculated as

$$^{EESI-TOF}SNR_{\alpha,j} = \frac{SMF_{\alpha,j}^{final}}{\sigma_{\alpha,j}^{SMF,final}}. \quad (14)$$

To retain only ions with a better SNR distribution than contaminant ions, we used a technique based on quantile-quantile plots (Q-Q plots). Contaminant ions are the measured ions coming from the species that spontaneously deposited on the field blank filters without pump aid, and are assumed to be present in all filters. The contaminant ions were considered to be the 5% of ions with highest signal in the field blanks, that is, with the highest $avg_{\alpha\epsilon FB}(SMF_{\alpha,j}^{final})$ (49 ions). The quantiles (from 10th to 90th in steps of 10) of all contaminant peaks' time series combined (merging all time series into a single array) were calculated and used as a reference for comparison to other ions, as shown with a black line in Fig. 2a. The same quantiles were calculated for the SNR time series of each ion (examples in Fig. 2a). Linear fits were performed on the Q-Q plots between each ion's SNR quantiles and the reference quantiles found for the field blanks' contaminant ions (example shown in Fig. 2b). In order to retain only the ions with consistently higher SNR

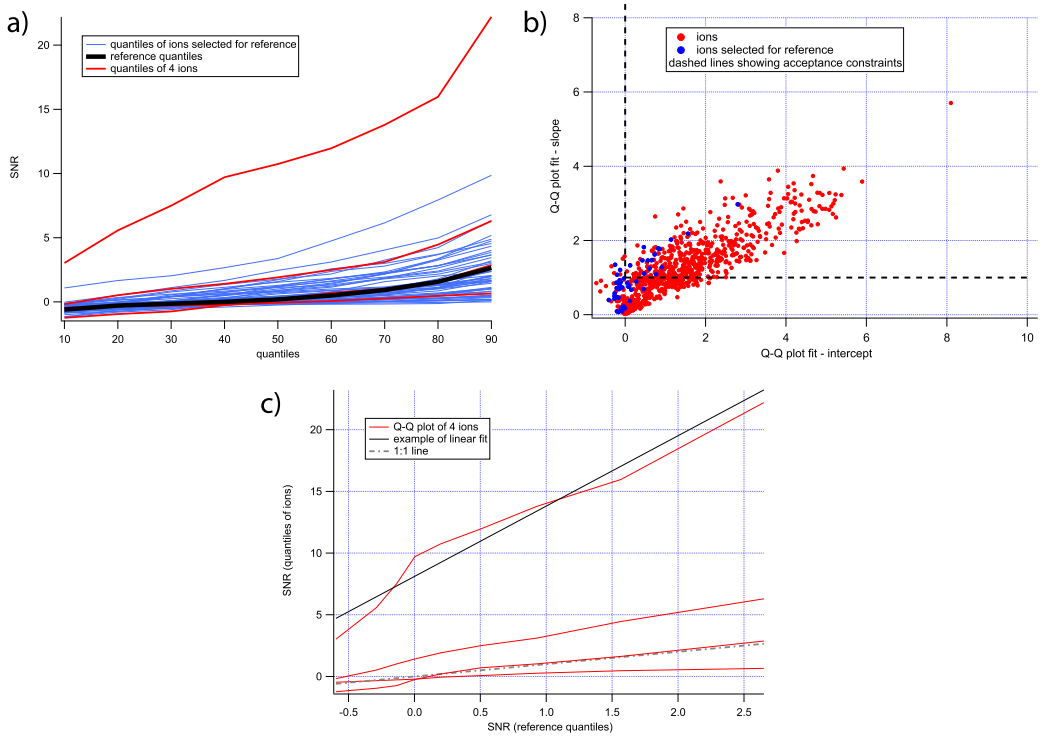

Fig. 2. Q-Q plot analysis. Plot (a) shows the SNR quantiles of the reference (in black), of the single contaminant ions that compose the reference (in blue), and of four sample ions (in red). Plot (b) shows the scatter plot of the fit parameters obtained by fitting the Q-Q plot of each single ion. Plot (c) shows the Q-Q plot of the same four sample ions in comparison to the contaminant ions reference quantiles, with an example of linear fit result. The blue points represent the contaminant ions. Only ions on the upper right side of the dashed lines in (b) are retained for further analysis. (For interpretation of the references to color in this figure legend, the reader is referred to the Web version of this article.)

for all quantiles with respect to the contaminant ions, we discarded all ions that yielded a fit with either a slope lower than 1, or an intercept lower than 0. Fig. 2c shows the resulting fit parameters for each ion, where the highlighted blue markers represent the contaminant ions.

Based on this approach, 473 of the initially 974 ions were retained for further analysis. The ions detected with the EESI-TOF were of two kinds, either $[M]Na^+$ (93% of total) or $[M]H^+$ (7% of total, 17.8% of the raw signal). The ions are listed as their corresponding compounds M of atmospheric relevance throughout the manuscript.

2.6. Source apportionment

Positive Matrix Factorization (PMF) is a bilinear receptor model with a non-negativity constraint (Paatero, 1999) used to separate the data matrix **X** into different sources. In this study, **X** represents the time series of AMS OA mass spectra from filter extracts. The equation used for the model is $\mathbf{X} = \mathbf{GF} + \mathbf{E}$, where **X** is the original data matrix of dimension $n \times m$, n being the number of time points and m the number of ions, **G** is the time-dependent contribution matrix of dimensions $n \times k$, where k is the parameter defining the number of factors in which to separate the matrix **X**, **F** is the factor profile matrix of dimensions $k \times m$, and **E** is the residual error of the bilinear fit. Both **F** and **G** are constrained to have non-negative elements. In practice, the system of equations is solved by minimizing the quantity Q using a gradient descent optimization:

$$Q = \sum_{\alpha, j} \left(\frac{e_{\alpha j}}{\sigma_{\alpha j}} \right)^2, \quad (15)$$

where $e_{\alpha j}$ are the elements of **E**, and $\sigma_{\alpha j}$ are the errors associated to each measurement. Optimization continues until a pre-set number of iterations fails to yield a further decrease in Q (i.e., convergence) or the maximum iteration count is reached (non-convergence). Here, PMF is implemented in the multilinear engine (ME-2) (Paatero, 1999), with model configuration and post-analysis performed in the Source Finder (SoFi v. 6.E, Datalystica Ltd.) toolkit (Canonaco et al., 2013, 2021).

In this study, each time-point in the **X** matrix represents a single 48-h filter quantified and field-blank subtracted HR-ToF-AMS spectrum obtained as described at the end of Section 2.4. The number of total AMS ions considered after SNR selection is 206. The total number of filters considered for PMF is 147. First, preliminary runs were performed to determine the number of factors and obtain an acceptable preliminary solution as a base case. Second, sensitivity tests were performed to investigate the PMF solution's uncertainty via bootstrapping the PMF inputs (Canonaco et al., 2013; Daellenbach et al., 2017, 2018). Finally, recoveries from WSOA to OA were estimated to confirm the physical acceptability of the solution and to estimate the total organic aerosol concentration for each single factor. Details regarding the number of factors, uncertainties assessment and recovery of water solubility values of each factor are described in the Supplementary material.

3. Results and discussion

3.1. Recoveries

Fig. 3a shows the retrieved recoveries of all factors using the random walk optimizer explained in the Supplementary material. The modelled OC agrees well with the measured OC, except for a peak consisting in 5 filters sampled in the end of January 2016 (starting dates of 22., 24., 26., 28., and 30.01.2016) which deviate from the measured OC (Fig. 3b).

3.2. OA sources

The average AMS solution from the bootstrapped inputs is presented in Fig. 4 and Fig. 5. All the following results are based on the average bootstrapped AMS OA source apportionment results, unless stated otherwise. Fig. 4 displays the chemical composition (factor profiles) of

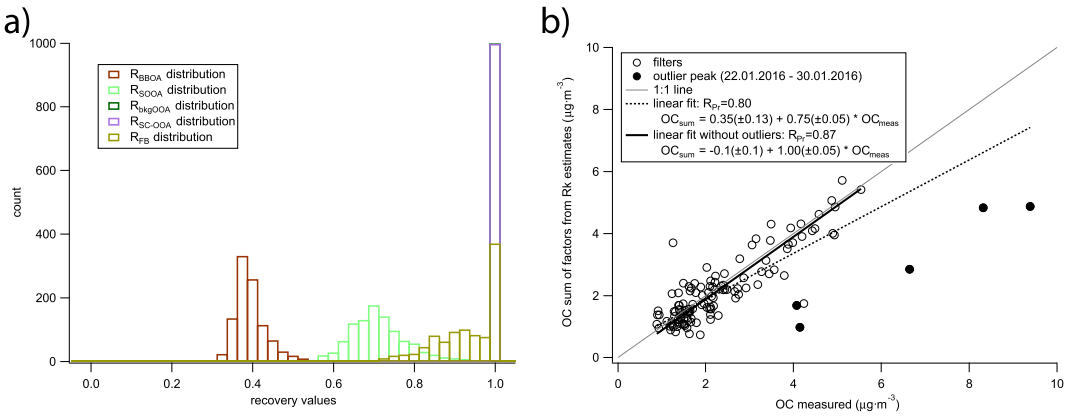

Fig. 3. Plot (a) shows the distribution of the recovery values found at the end of each of the 1000 random walks. The distributions of R_{bkgOOA} and $R_{SC\text{-}OOA}$ are overlapping in 1 and thus impossible to distinguish. Plot (b) shows the scatter plot of the total modelled OC, obtained by correcting the WSOC for factors and FB, against the measured OC. The two fits show the agreement between the OC values, calculated for (1) all data (all circles and dashed line) and (2) without 5 outlier filters from January 2016 (empty circles and solid line) which do not seem to be appropriately explained by the recoveries. (For interpretation of the references to color in this figure legend, the reader is referred to the Web version of this article.)

the 4 factors. In Fig. 5, the factor time series are presented alongside meteorological observations as well as other PM constituents. In Fig. 6 scatter plots of the factor time series against temperature are shown. Detailed comparisons between the OA sources' temporal variability with collocated analyses (Spearman correlation coefficient matrix) are presented in Fig. 7.

3.2.1. Primary OA

The first factor is designated as primary biomass burning OA (BBOA). This source is characterized by high contributions of the typical markers at *m/z* 60 ($C_2H_4O_2^+$) and 73 ($C_3H_5O_2^+$) (Fig. 4) and overall resembles the chemical fingerprint of BBOA from previous field and laboratory studies as well as nebulized levoglucosan – a major constituent of fresh wood burning emissions (Alfarra et al., 2007; Bozzetti et al., 2017a; Bruns et al., 2016; Crippa et al., 2014; Daellenbach et al., 2017; Kostenidou et al., 2013; Mohr et al., 2015; Schneider et al., 2006). Although the profile shows a high contribution from the fragment ion CO_2^+, its share in the normalized bootstrapped profile is highly uncertain (0.1 ± 0.1), and does therefore not contradict the interpretation of this factor being relatively fresh and of rather local origin. In addition, the BBOA time series correlates with that of the EESI-TOF measurement of $C_6H_{10}O_5$ (corresponding to levoglucosan and its isomers), as shown in Fig. 5 ($R_{Sp} = 0.87$). Previous EESI-TOF studies showed this compound to be strongly enhanced in fresh primary BBOA emissions (Qi et al., 2019; Tong et al., 2021). BBOA relative concentrations are 2.4 times higher during the cold period ($T < 15$ °C) compared to 20–25 °C average temperatures (2.1 times enhanced as absolute concentration). BBOA concentrations increase when temperatures fall below 17 °C, as well as when temperature increases above 25 °C (Fig. 6a). This behavior was attributed to the onset of biomass burning used for heating at low temperatures, and the onset of wild and/or controlled fires during the warm period (Cvitešić Kušan et al., 2020). This is also in agreement with the air mass transport from regions with active wildfires as indicated by backward trajectories (Figs. S13, S14, and S15).

3.2.2. Secondary OA

Three oxygenated OA (OOA) factors were identified by distinct chemical compositions and temporal behaviors.

Background oxygenated OA (bkgOOA) is the most oxygenated factor retrieved (O:C = 1.1), with CO_2^+ contributing 25 ± 6% of the total factor mass (Fig. 4), confirming a high contribution of organic acids of secondary origin in the analyzed samples (Cvitešić Kušan et al., 2020; Duplissy et al., 2011). The bkgOOA concentration does not show a strong seasonal cycle and correlates with SO_4^{2-} ($R_{Sp} = 0.55$) and oxalate ($R_{Sp} = 0.59$), indicating aged and possibly long-range transported anthropogenic SOA. The naming of the factor follows the nomenclature of Bozzetti et al. (2017b) for regional OOA. However, during the late summer months the concentration is enhanced, following the increase in temperature (Fig. 6c). This is consistent with the increase in BBOA concentrations and might be related to SOA formation from transported wildfire emissions (Bougiatioti et al., 2014; Kodros et al., 2020; Zhou et al., 2017). Analysis of fire maps and back-trajectories (see Figs. S13, S14, S15) show these to be present especially in the Ukraine region during the warm season and even extending to autumn (ORNL, 2017), in addition to local open-fire episodes close to the sampling site during summer 2016 as previously described in Cvitešić Kušan et al. (2020). Worth mentioning is also the simultaneous increase of the fractions of SO_4^{2-} and bkgOOA in $PM_{2.5}$ from the cold to the warm period, with SO_4^{2-} increasing from 15% to 26% and bkgOOA from 14% to 19% as seen in Fig. 8.

Summer oxygenated OA (SOOA) is the least oxygenated of the OOA factors (O:C = 0.57). Besides, the CO_2^+ fraction apportioned to this factor is very uncertain (0.1 ± 0.2). Fig. 6 shows that the SOOA concentration increases exponentially with local temperature, consistent with previously observed biogenic SOA formation (Bozzetti et al., 2017a; Daellenbach et al., 2017, 2019; Guenther et al., 1995; Leaitch et al., 2011; Vlachou et al., 2018, 2019). The chemical profile of SOOA in Fig. 4 also shows characteristics of biogenic SOA, in particular, a prominent contribution of the peaks at *m/z* 82 (composed almost entirely of $C_5H_6O^+$) and *m/z* 53 (composed of $C_4H_5^+$) consistent with both online and offline studies of OA (Chen et al., 2015; Daellenbach et al., 2017; Kostenidou et al., 2015; Vlachou et al., 2019; Xu et al., 2015). We found a 3.4 fold increase of SOOA contribution to OA (2.3 fold increase in contribution to $PM_{2.5}$) in the warm season as compared to the cold season (Fig. 8), in line with the increasing local temperature and solar radiation and thus biological activity in the sea surface layers as well as on the continent as important natural emission source.

Sulfur-containing oxygenated OA (SC-OOA) is characterized by a high contribution of the organosulfur fragments $CHSO^+$ (100%) and $CH_3SO_2^+$ (100%) and is highly oxygenated (O:C = 1). However, the sensitivity analysis shows also for this factor a highly uncertain apportionment of the CO_2^+ signal of 0.07(±0.10). SC-OOA shows a time series that is rather inconsistent and unpredictable (Fig. 5), suggesting it could depend strongly on the air mass origin and specific events. It is also striking that the SC-OOA is not influenced by temperature, even though the time series of the factor shown in Fig. 5 displays higher values in the second year of the sampling campaign. Despite of similar features, it is improbable that SC-OOA represents non-exhaust traffic emissions as

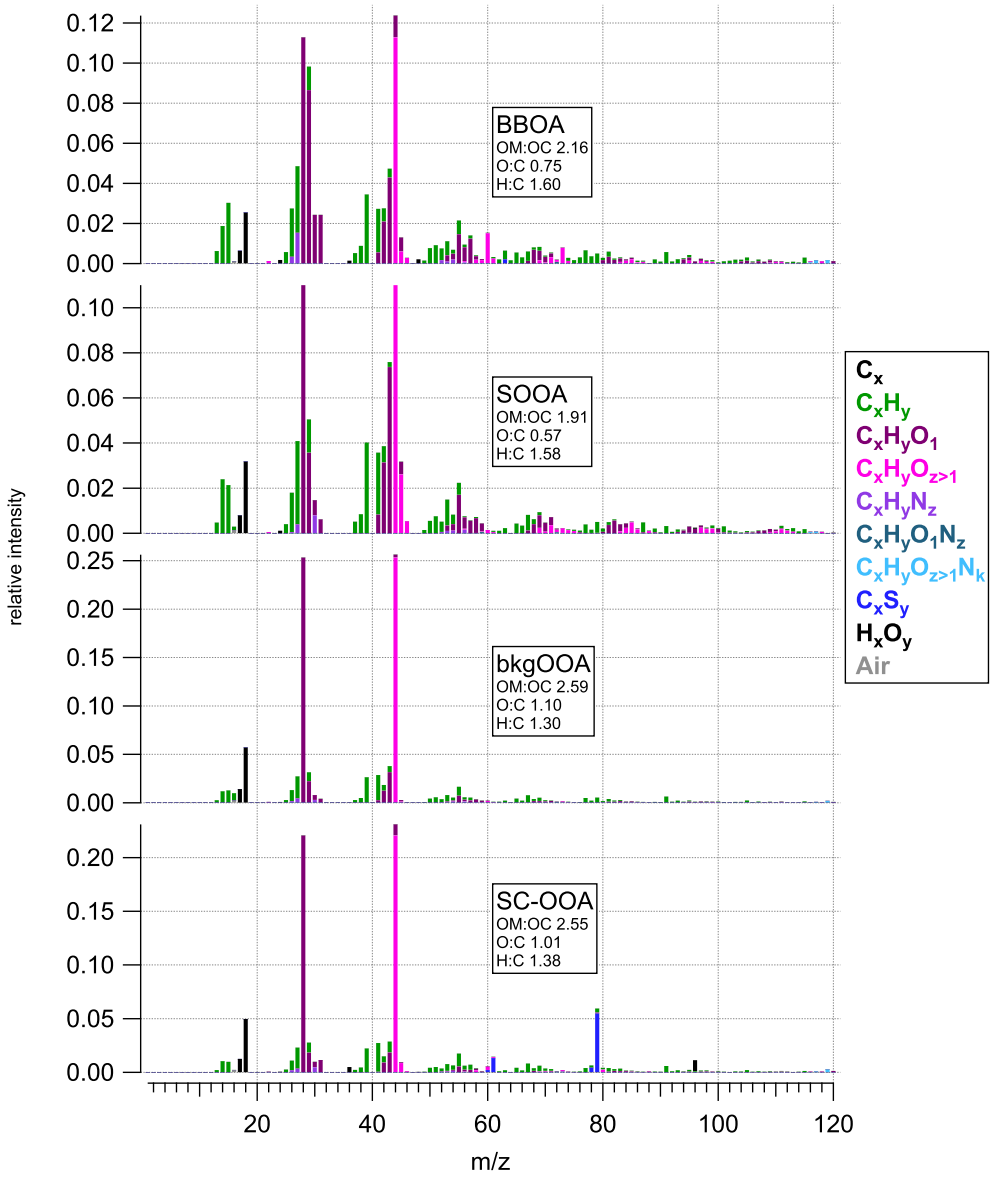

Fig. 4. Factor profiles of OA sources from AMS source apportionment. The colors codify the different families of chemical species found in the legend. (For interpretation of the references to color in this figure legend, the reader is referred to the Web version of this article.)

found at other locations (Daellenbach et al., 2017, 2020; Vlachou et al., 2018) because such mechanically generated particles are predominantly found in coarse PM, whereas here $PM_{2.5}$ is measured. Although a small portion of such traffic related PM might also fall within $PM_{2.5}$, reasonably constant concentration of such a factor is anticipated throughout the year and between successive years, which is inconsistent with our data. The correlation table in Fig. 7 shows that this factor does not correlate significantly with any of the supplemental data. It is also noteworthy that SC-OOA does not correlate with methane sulfonic acid (MSA) (Fig. S9g). Since MSA is formed from marine dimethylsulfide (DMS) emissions (Crippa et al., 2013), the inconsistent temporal behavior of the two time series suggests that SC-OOA is not directly related to marine biogenic emissions. However, this factor also does not correlate well with either the total PM mass, NO_3^-, SO_4^{2-} – either non-sea-salt related SO_4^{2-} or biogenic non-sea-salt related SO_4^{2-} (Fig. S9). In 2016, the high SC-OOA concentrations occurred in spring and autumn consistent with spring and autumn vertical instability of the lake water column stratification (Čanković et al., 2020). During lake mixing, sulfide-like compounds were detected in WSOC in a previous study (Cvitešić Kušan et al., 2019) highlighting the strong presence of atmospheric sulfur in line with high SC-OOA concentrations. In 2015 the Rogoznica lake was more strongly stratified than in 2016 (unpublished data, MARRES project), in line with higher emissions during 2016 (Cvitešić Kušan et al., 2019). Therefore, we hypothesize that emissions from the Rogoznica Lake - up to 5 m from the sampling location - could be one of the main source of SC-OOA. However, the possible long-range transport of SO_2 forming organosulfates cannot be completely ignored either.

3.3. Source contributions to OA and PM

For further interpretation we separated the obtained data into warm and cold periods, respectively defined as 48-h average temperatures during sampling above or below 15 °C (warm: 100 filters, cold 43 filters).

The pie charts in Fig. 8a and b shows the relative PM composition during the cold and warm periods. Secondary inorganic aerosol (SIA) in summer is largely composed of SO_4^{2-}, comprising 26% of the measured

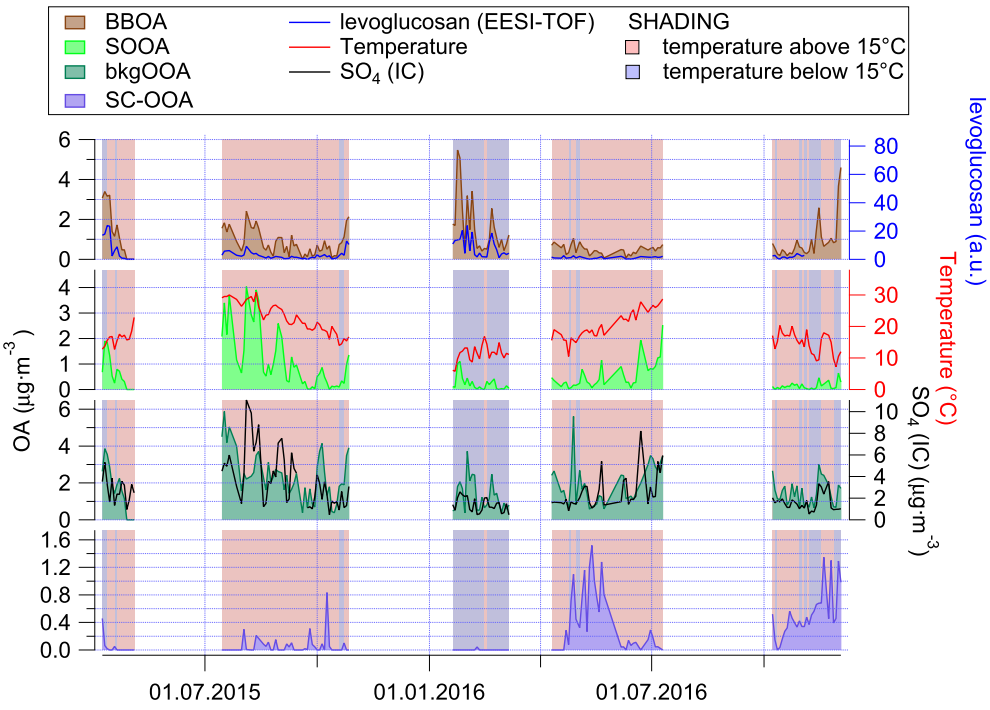

Fig. 5. Time series of OA components from AMS source apportionment after recovery correction. The temperature time series is shown in the SOOA plot, since this factor correlates best with temperature. The time series of levoglucosan (from EESI-TOF) and sulfate are also plotted for comparison. The red and blue shading corresponds to the periods in which the average temperature over the two sampling days was above or below 15 °C, respectively. (For interpretation of the references to color in this figure legend, the reader is referred to the Web version of this article.)

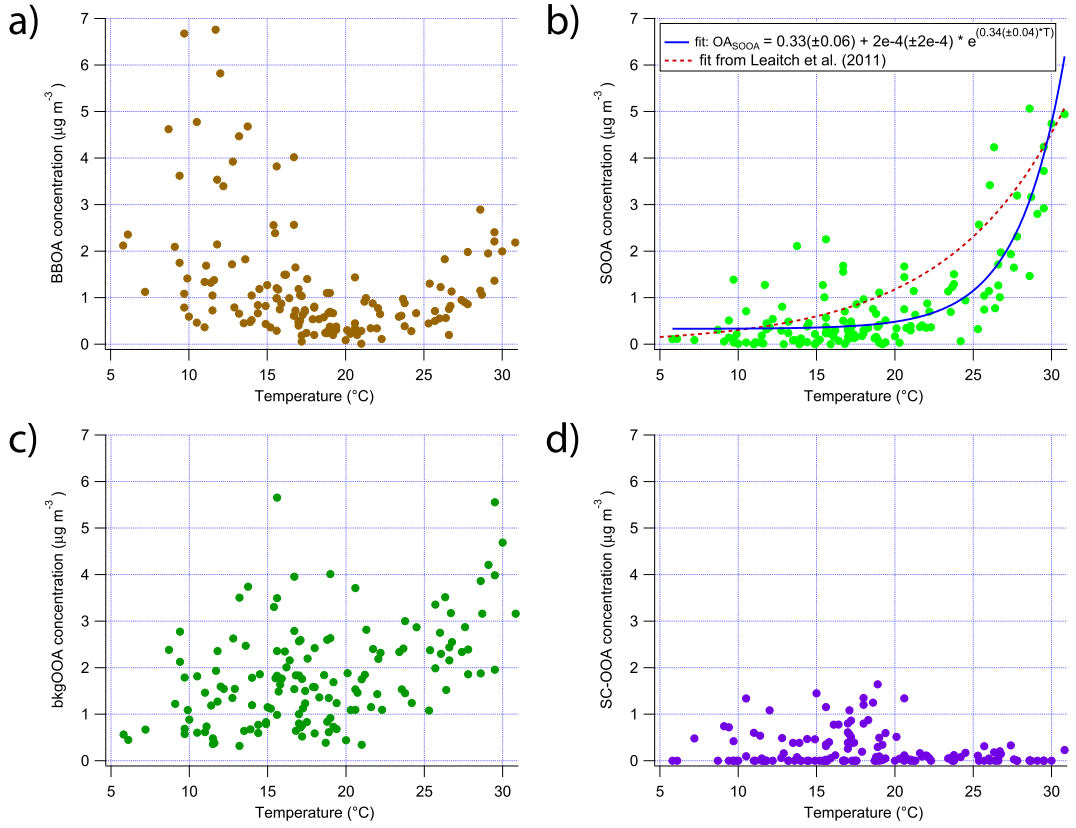

Fig. 6. Scatter plots of (a) BBOA, (b) SOOA, (c) bkgOOA, and (d) SC-OOA concentration vs. average temperature over the sampling time. The exponential fit performed for the SOOA yielded $OA_{SOOA} = 0.33(\pm0.06) + 0.0002(\pm0.0002) \cdot \exp(0.34(\pm0.04) \cdot T)$, and the fit from Leaitch et al. (2011) is displayed for comparison.

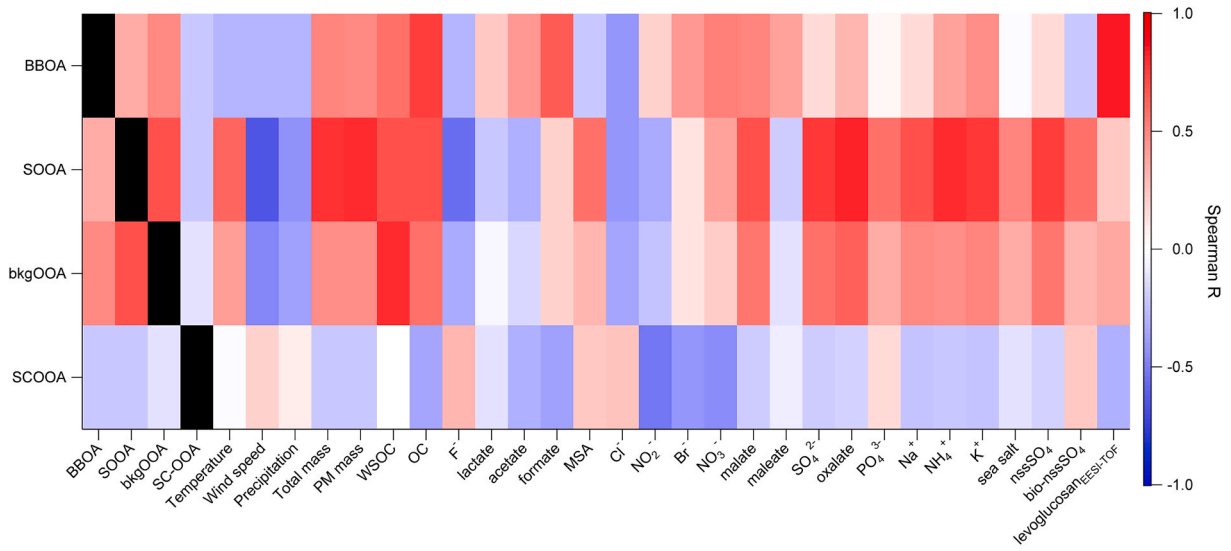

Fig. 7. Spearman correlations between factor time series and supporting data. The levoglucosan was obtained from the EESI-TOF measurements. The nssSO_4 and the bio-nssSO_4 were obtained following Cvitešić Kušan et al. (2020) and Millero (2013). (For interpretation of the references to color in this figure legend, the reader is referred to the Web version of this article.)

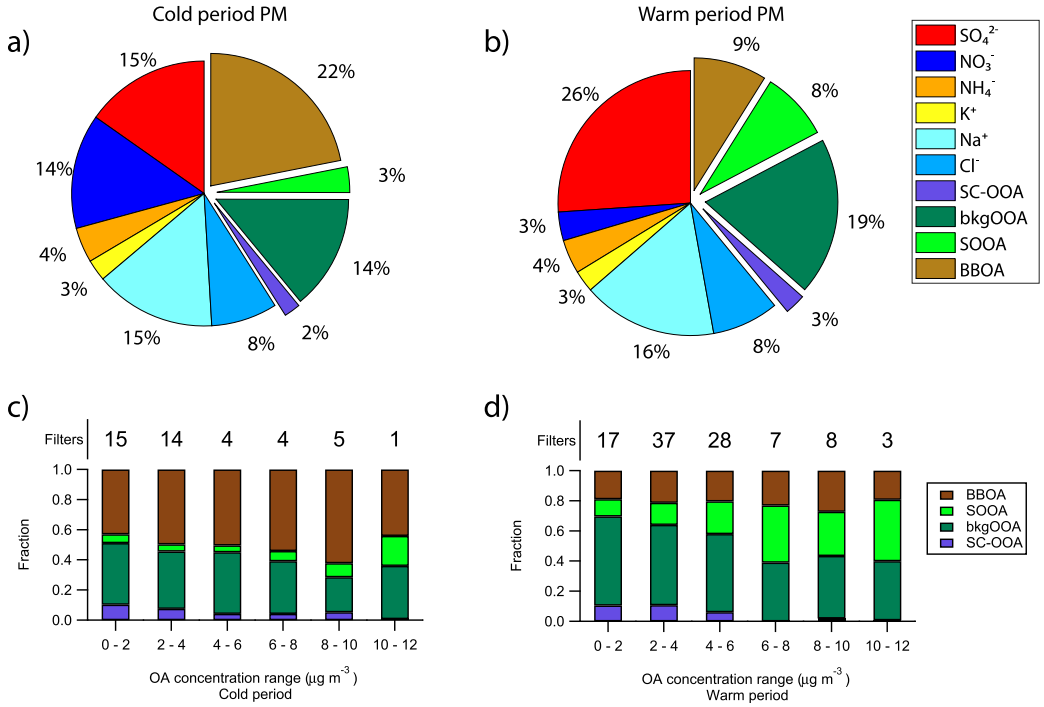

Fig. 8. Chemical composition of $PM_{2.5}$ in Rogoznica, Crotia: (a) cold period, (b) warm period. The SC-OOA, bkgOOA, SOOA and BBOA refer to the OA concentrations obtained from the AMS PMF analysis. Drivers of OA pollution in Rogoznica, Croatia: Relative contributions of AMS-related PMF factors to OA during (c) the warm period and (d) the cold period. Warm/cold periods were defined as 48-hr sampling periods with temperatures above/below 15 °C. The number of filters that fall under the corresponding OA concentration for each period are shown above each bar. (For interpretation of the references to color in this figure legend, the reader is referred to the Web version of this article.)

aerosol concentration, while the cold period exhibits an equal contribution of SO_4^{2-} and $NO_3^-$of around 15%. High NO_3^- contribution in cold-period samples can be attributed to combustion sources, and are further enhanced by increased partitioning of ammonium nitrate to the particle phase during the cold period due to the lower temperatures. On the other hand, SO_4^{2-} is due to enhanced photooxidation in the case of warm-period samples. The contributions of the other inorganic aerosol constituents do not change substantially, the second biggest contribution being that of sodium, typical of a coastal location.

OA contributes roughly 40% to $PM_{2.5}$ during both the warm and cold periods, but the contributions of OA sources vary seasonally. The cold period is characterized by a higher contribution of BBOA to total OA (53%, 22% to PM) than during the warm period (30%, 9% to PM), which is consistent with higher NO_3^- contribution. It is thus plausible that during winter/in colder days BBOA is related to residential heating and/or open fires (e.g. agricultural waste). However, during summer/on

warmer days wildfires may play the major role, since in the coastal region waste burning is forbidden in this time of a year. The overall biggest contributor to organic aerosol is bkgOOA, comprising 44% of the OA and 18% of the PM mass throughout the year, with a slightly higher contribution to OA in the warm period (48%, 19% to PM) than in the cold period (44%, 14% to PM). In Crete, i.e. further south in the eastern Mediterranean, a highly oxygenated aerosol similar to the bkgOOA factor was dominating the total aerosol at that site (Hildebrandt et al., 2010). In contrast to Crete, other organic fractions are important as well at the coast of Croatia. SOOA is only a minor contributor to OA during the cold period (7%, 3% to PM) but a major contributor during the warm period (24%, 8% to PM), consistent with increased emissions of biogenic SOA precursors at higher temperatures. SC-OOA is a minor contributor to OA (6%, 2% to PM) both during the warm and cold seasons. In fact, SC-OOA is not influenced by the season, without a clear dependence on the temperature. Generally, aged OOA/SOA found in the Mediterranean dominates the OA, e.g., Bozzetti et al. (2017a) found a 55% contribution of OOA to OA in Marseille, France, during the summer and Kostenidou et al. (2015) found a 65% contribution of OOA to OA in Patras and Athens, Greece, during the summer. The total OOA contribution to OA found in this work was 77% during the warm period.

The bar plots in Fig. 8c and d display the OA fractional contributions of the retrieved OA factors during the cold and warm periods, respectively, as a function of the total OA mass. During the cold period, increasing OA levels correspond to the increasing fraction of BBOA, which shows the big influence the local biomass burning from residential heating has on the OA concentration during winter. The warm period is instead characterized by a stable fraction of BBOA as well as an increasing fraction of SOOA with increasing OA concentration in the atmosphere, pointing to SOOA being a major driver of OA pollution in summer.

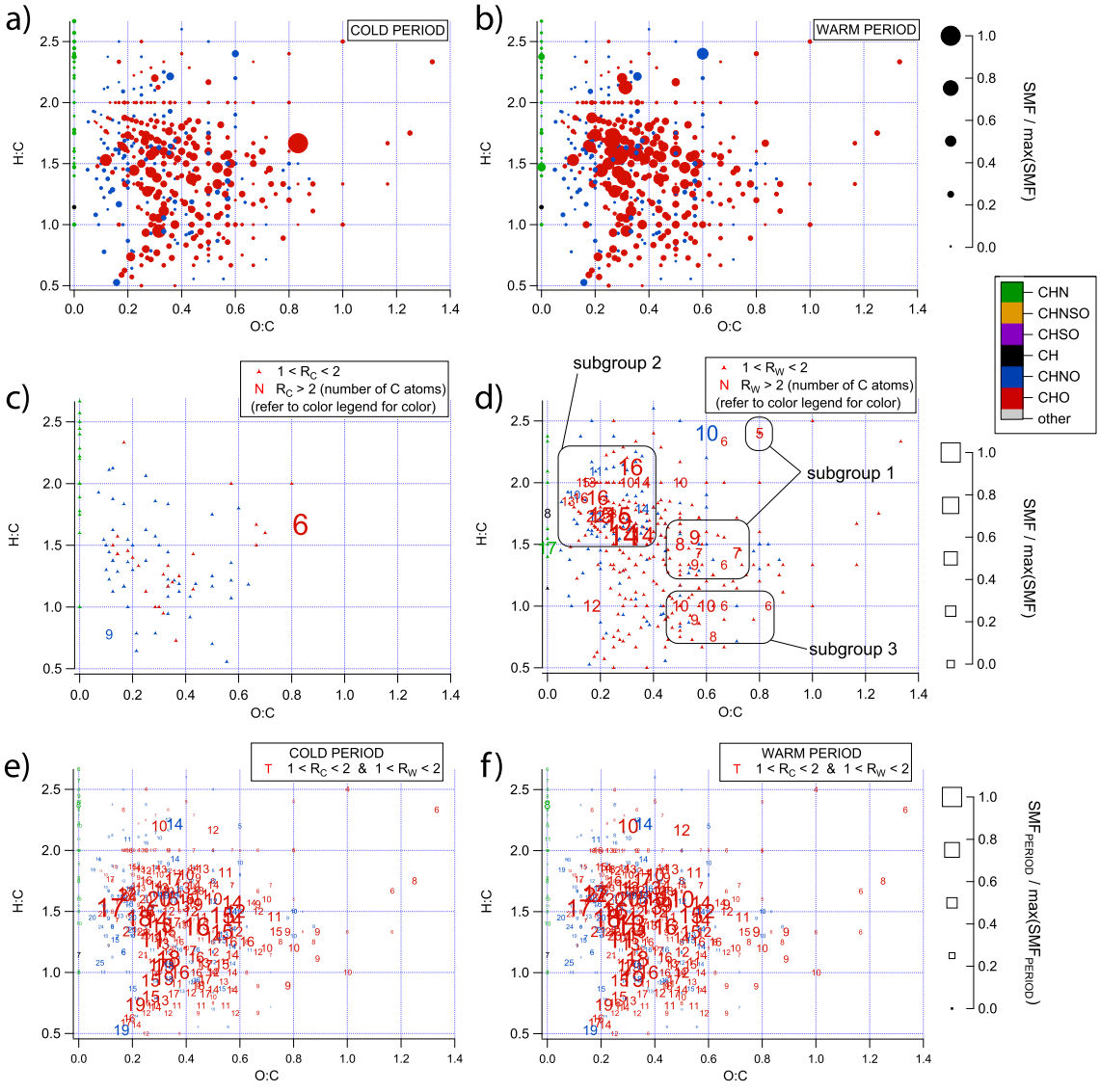

Fig. 9. Atomic H:C ratio as a function of O:C ratio (van Krevelen diagrams). Plots (a) and (b) show all compounds with symbol size depending on the (a) average SMF during cold period (SMF_{COLD}) and (b) average SMF during warm period (SMF_{WARM}) compared to the maximum of the respective period. Van Krevelen diagrams displaying the carbon number of the compounds with $R_C > 2$ (c) and of the compounds with $R_W > 2$ (d), with number sizes proportional to SMF_{COLD} and SMF_{WARM}, respectively, together with the other compounds satisfying $1<R_C < 2$ (c) and $1<R_W < 2$ (d); see text for explanation of subgroups. Plots (e) and (f) both show the carbon atom number of compounds with $1<R_C < 2$ and $1<R_W < 2$, with number sizes proportional to SMF_{COLD} and SMF_{WARM}, respectively. All markers and numbers displayed are colored based on molecular formula as shown in the color legend. All symbol and number sizes are normalized to the highest SMF among the ones present in each plot. (For interpretation of the references to color in this figure legend, the reader is referred to the Web version of this article.)

3.4. EESI measurements – molecular composition by season

Fig. 9 presents the EESI-TOF measurement of OA composition during the cold (Fig. 9a-c-e) and warm periods (Fig. 9b-d-f) as plots of H:C versus O:C (van Krevelen diagrams). Fig. 9a–f displays the compounds grouped and colored by molecular formula. The compounds' symbols are sized proportionally to the average specific mass flux *SMF* defined in Equation (13), during the cold period SMF_{COLD} (Fig. 9a) and during the warm period SMF_{WARM} (Fig. 9b) normalized to the highest *SMF* value among the ones displayed in the respective plot. $C_8H_{18}O_5$ is the most abundant compound both during the warm and cold season. While this compound was found in a factor that was tentatively related to diverse sources (e.g. cooking, plastic burning, Qi et al. (2019)), we cannot exclude it as a contaminant (e.g. tetraethylene glycol) even if the compound was detected at much higher rates for samples than field blanks. For caution, this ion was removed for further analysis and is not displayed in Fig. 9. Fig. 9c and d help visualizing which compounds are enhanced more than two-fold with respect to the opposite period, as calculated in Equations (19) and (20).

$$R_C := \frac{SMF_{COLD}}{SMF_{WARM}} > 2 \tag{19}$$

$$R_W := \frac{SMF_{WARM}}{SMF_{COLD}} > 2 \tag{20}$$

Seasonally enhanced compounds are shown as numbers (denoting carbon number), and the sizing of the carbon number is proportional to SMF_{COLD} and SMF_{WARM} of the respective compound, normalized to the highest *SMF* value among the ones displayed in the respective plot. Fig. 9c and d also display the compounds with R_C and R_W, respectively, between 1 and 2, i.e. compounds that only exhibit a moderate seasonal variability. These are also shown together (with their carbon number) in Fig. 9e and f for better viewing, sized with the same ratio as in Fig. 9a and b.

In general, the molecular composition during the cold and warm period is strikingly similar (Fig. 9a and b), with only a few compounds exhibiting $R_C > 2$ or $R_W > 2$ (Fig. 9c and d). Thus the bulk SOA appears to have a similar composition during the warm and cold period. This is consistent with the high contribution of bkgOOA to OA and SOA during both periods (warm: 48% of OA and 62% of SOA, cold: 34% of OA and 72% of SOA). Most of the low concentration compounds in the C10–C18 range exhibit similar concentration ratios with the high concentration compounds in both periods, hinting to the fact that these compose the bulk of the bkgOOA factor. An exception is found for a few compounds in the range of C13–C20, H:C = 1–1.5, and O:C = 0.2–0.6 which in the cold period have a higher concentration with respect to the other seasonally independent compounds.

Fig. 9c shows that during the cold period $C_6H_{10}O_5$ (presumably mostly levoglucosan) is the only compound with $R_C > 2$ as well as a high *SMF* of 7.8 *ag/s* (for comparison, the highest *SMF* among compounds with $R_W > 2$ is 8.7 *ag/s*). This is in line with the 2.4 times higher BBOA concentration during the cold compared to the warm period in relative terms. The only other compound satisfying $R_C > 2$ condition is C_9H_7NO, which however does not have a high *SMF* and is thus not a major contributor to (S)OA mass. During the warm period there are considerably more compounds with $R_W > 2$ (38 out of the 377 compounds with higher concentration in the warm period, Table S4), with three subgroups of particular interest. The first subgroup contains compounds with carbon numbers from 5 to 10, with an O:C ratio around 0.5, and an H:C ratio around 1.5 (e.g. $C_7H_{10}O_4$, $C_8H_{12}O_4$, $C_9H_{12}O_5$, $C_9H_{14}O_5$). These molecular formulas are consistent with those of previously reported monoterpene oxidation products (Claeys et al., 2013; Mutzel et al., 2016; Ye et al., 2018), for example terebic acid ($C_7H_{10}H_4$), and norpinic and/or terpenylic acids ($C_8H_{12}O_4$), and consistent with the major ions in the biogenic SOA profiles resolved from recent online and offline EESI-TOF studies in Zurich, Switzerland ($C_7H_{10}O_4$, $C_7H_{10}O_5$, $C_9H_{14}O_5$, $C_9H_{12}O_5$) (Stefenelli et al., 2019; Qi et al., 2019, 2020). In addition, $C_5H_{12}O_4$ can be associated with the major biogenic SOA products of 2-methyltetrols (2-methylthreitol and 2-methylerythritol) derived from (Claeys et al., 2004). The second subgroup consists of compounds with an O:C ratio close to 0.3 and an H:C ratio close to 1.7. It includes compounds with higher carbon number, such as $C_{14}H_{22}O_5$, $C_{14}H_{22}O_4$, $C_{15}H_{26}O_4$, $C_{19}H_{32}O_5$, and $C_{14}H_{25}NO_5$. These C14–C15 formulas ($C_{14}H_{22}O_4$, $C_{14}H_{22}O_5$, $C_{14}H_{28}O_5$) are tentatively identified as sesquiterpene oxidation products, which are still consistent with those previously identified in the biogenic SOA profile from offline EESI measurements (Qi et al., 2020). These observations indicate common biogenic sources (VOCs such as isoprene, monoterpenes, and sesquiterpenes) and potential regional transport in summer. This group also includes compounds with higher carbon number that might be oxidized products of alkanes, SOA precursors of anthropogenic origin, such as traffic emissions from motor oil and diesel fuel or cooking emissions (Calvert et al., 2008; Platt et al., 2014). The third subgroup is composed of compounds characterized by an O:C ratio of around 0.6 and an H:C ratio around 1 (e.g. $C_6H_6O_4$, $C_8H_6O_5$, $C_9H_8O_5$, $C_{10}H_{10}O_5$, $C_{10}H_{10}O_6$). Given the low H:C ratio, it is likely that these compounds originate from aromatic precursors of anthropogenic origin, such as benzene, trimethylbenzene, vanillin, and naphthalene.

4. Conclusions

We successfully performed a source apportionment of the OA fraction of $PM_{2.5}$ samples collected during two years at a coastal site of the Eastern Adriatic Sea (Rogoznica, Croatia). The filtered water extracts were nebulized and measured with an aerosol mass spectrometer (HR-ToF-AMS) and used for apportioning OA to its sources using the positive matrix factorization (PMF) algorithm. Four factors were identified, of which one was linked to primary aerosol (biomass burning OA, BBOA) and three to secondary OA (summer oxygenated OA, SOOA; background oxygenated OA, bkgOOA; and sulfur-containing oxygenated OA, SC-OOA). BBOA is characterized by the typical markers at *m/z* 60 ($C_2H_4O_2^+$) and 73 ($C_3H_5O_2^+$). The time series of the factor correlates with $C_6H_{10}O_5$ (from the EESI-ToF, $R_{Sp} = 0.87$), which is likely dominated by levoglucosan. During the cold period BBOA is thought to be dominated by residential heating emissions, while the increase in BBOA concentrations at temperatures above 25 °C is consistent with abundant local and regional (Eastern Europe) wildfire emission. Second, SOOA is characterized by elevated concentrations during warmer periods, consistent with biogenic SOA formation. The bkgOOA factor is characterized by a high concentration throughout the campaign, and the highest oxygenation among the factors (O:C = 1.1). It correlates with secondary inorganic aerosol constituents, such as SO_4^{2-} ($R_{Sp} = 0.55$), as well as with $C_2O_4^{2-}$ ($R_{Sp} = 0.59$), suggesting that long-range transported anthropogenic VOC emissions are an important contributor to regional SOA. During the warm period, the bkgOOA concentration is enhanced at higher temperatures. The increase in bkgOOA coincides with abundant local and/or regional wildfires, suggesting that SOA from wildfire emissions might contribute to the increase. Finally, SC-OOA is characterized by a high contribution of the ions *m/z* 61 ($CHSO^+$) and 79 ($CH_3SO_2^+$), which fully apportion to this factor. Despite $CHSO^+$ and $CH_3SO_2^+$ being typically used as markers of marine biogenic SOA, the lack of a correlation between SC-OOA and MSA suggests that SC-OOA is not directly related to marine biogenic emissions. We hypothesize that the most likely source of such emissions is the Rogoznica marine lake, which emits sulfur compounds when the vertical stability of the water column stratification is perturbed. The possible long-range transport of SO_2 might also contribute to the factor to a lower degree.

Molecular characterization of the OA composition performed with a soft-ionization EESI-TOF-MS contributed to a deeper understanding and characterization of some of the sources. The analysis shows strong enhancement of the biomass burning-tracer levoglucosan during the cold period. In fact, the average concentrations of most compounds do

not change drastically between the cold and warm periods. This is consistent with bkgOOA as a main contributor to OA throughout the year. Based on the molecular characterization, diverse precursor emission sources presumably contribute to bkgOOA. During the warm period, two groups of compounds are mostly enhanced. The first group displays the characteristics of oxidation products of biogenic monoterpenes (e.g. $C_8H_{12}O_4$, $C_9H_{14}O_5$, $C_7H_{10}O_4$, $C_9H_{12}O_5$), which is in line with the interpretation of SOOA as biogenic SOA. The second group could be composed of fragments of oxidized alkanes (e.g. $C_{14}H_{22}O_5$, $C_{14}H_{22}O_4$, $C_{15}H_{26}O_4$, $C_{19}H_{32}O_5$, and $C_{14}H_{25}NO_5$) and oxidized aromatic compounds ($C_6H_6O_4$, $C_8H_6O_5$, $C_9H_8O_5$, $C_{10}H_{10}O_5$, $C_{10}H_{10}O_6$), presumably of anthropogenic origin.

The complexity and challenges faced with finding a correct OA source apportionment and the data presented in this work show the importance of pursuing such projects and presenting datasets of such non-urban and less-polluted marine environments, as they are key to understanding the global influence of anthropogenic aerosol and their impact on climate change, human health, and the marine environment.

Funding information

The authors acknowledge the financial support from the projects "The Sulfur and Carbon Dynamics in the Sea and Fresh-Water Environment" (IP-11-2013-1205 SPHERE), Slovenian research Agency (Contract No. P1-0034), STSM "Source apportionment study of fine organic aerosols in the Middle Adriatic area" funded by COST COLOSSAL Action (CA16109) and the Croatian-Slovenian bilateral project "Estimating the role of marine biogenic organosulfur compounds in the formation and properties of atmospheric organic aerosols." We also acknowledge the financial support of the SNF project IZLCZ2_169 986 (HAZECHINA).

CRediT authorship contribution statement

R. Casotto: Investigation, Methodology, Software, Data curation, Formal analysis, Writing – original draft, Writing – review & editing, Visualization. **A. Cvitešić Kušan:** Conceptualization, Formal analysis, Investigation, Writing – review & editing. **D. Bhattu:** Investigation, Writing – review & editing. **T. Cui:** Investigation. **M.I. Manousakas:** Software. **S. Frka:** Conceptualization, Funding acquisition, Investigation, Writing – review & editing, Project administration. **A. Kroflič:** Investigation, Writing – review & editing. **I. Grgić:** Resources, Writing – review & editing. **I. Ciglenečki:** Funding acquisition, Resources, Writing – review & editing. **U. Baltensperger:** Supervision, Writing – review & editing. **J.G. Slowik:** Supervision, Writing – review & editing. **K.R. Daellenbach:** Supervision, Conceptualization, Writing – review & editing. **A.S.H. Prévôt:** Supervision, Conceptualization, Project administration, Funding acquisition, Writing – review & editing.

Declaration of competing interest

The authors declare that they have no known competing financial interests or personal relationships that could have appeared to influence the work reported in this paper.

Acknowledgments

The Croatian Science Foundation projects IP-11-2013-1205 SPHERE, and IP-2018-01-1717 MARRES, for PMs sampling and TOC analyses, and respectively for data (discussion) on Rogoznica lake water column stratification and reduced sulfur species concentration. Also Marina Frapa Rogoznica has to be highly acknowledged for support during aerosol sampling. The author acknowledges the company Datalystica and Canonaco Francesco for the support with the SoFi Igor toolkit. Acknowledgements also to Imad el Haddad for the initial support, as well as Chuan Ping and Veronika Pospisilova for the initial support given with the EESI-TOF measuring campaign. We acknowledge the help given by Houssni Lamkaddam, Anna Tobler, David Bell, and Vaios Moschos for the source apportionment interpretation.

Appendix A. Supplementary data

Supplementary data to this article can be found online at https://doi.org/10.1016/j.aeaoa.2022.100159.

The data plotted in the figures and the PMF input matrix can be downloaded at https://doi.org/10.5281/zenodo.5599743.

References

Aiken, A.C., DeCarlo, P.F., Kroll, J.H., Worsnop, D.R., Huffman, J.A., Docherty, K.S., Ulbrich, I.M., Mohr, C., Kimmel, J.R., Sueper, D., Sun, Y., Zhang, Q., Trimborn, A., Northway, M., Ziemann, P.J., Canagaratna, M.R., Onasch, T.B., Alfarra, M.R., Prevot, A.S.H., Dommen, J., Duplissy, J., Metzger, A., Baltensperger, U., Jimenez, J. L., 2008. O/C and OM/OC ratios of primary, secondary, and ambient organic aerosols with high-resolution time-of-flight aerosol mass spectrometry. Environ. Sci. Technol. 42, 4478–4485.

Alfarra, M.R., Prevot, A.S.H., Szidat, S., Sandradewi, J., Weimer, S., Lanz, V.A., Schreiber, D., Mohr, M., Baltensperger, U., 2007. Identification of the mass spectral signature of organic aerosols from wood burning emissions. Environ. Sci. Technol. 41, 5770–5777.

Bougiatioti, A., Stavroulas, I., Kostenidou, E., Zarmpas, P., Theodosi, C., Kouvarakis, G., Canonaco, F., Prévôt, A.S.H., Nenes, A., Pandis, S.N., Mihalopoulos, N., 2014. Processing of biomass-burning aerosol in the eastern Mediterranean during summertime. Atmos. Chem. Phys. 14, 4793–4807.

Bozzetti, C., Daellenbach, K.R., Hueglin, C., Fermo, P., Sciare, J., Kasper-Giebl, A., Mazar, Y., Abbaszade, G., El Kazzi, M., Gonzalez, R., Shuster-Meiseles, T., Flasch, M., Wolf, R., Křepelová, A., Canonaco, F., Schnelle-Kreis, J., Slowik, J.G., Zimmermann, R., Rudich, Y., Baltensperger, U., El Haddad, I., Prévôt, A.S.H., 2016. Size-resolved identification, characterization, and quantification of primary biological organic aerosol at a European rural site. Environ. Sci. Technol. 50, 3425–3434.

Bozzetti, C., El Haddad, I., Salameh, D., Daellenbach, K.R., Fermo, P., Gonzalez, R., Minguillón, M.C., Iinuma, Y., Poulain, L., Elser, M., Müller, E., Slowik, J.G., Jaffrezo, J.L., Baltensperger, U., Marchand, N., Prévôt, A.S.H., 2017a. Organic aerosol source apportionment by offline-AMS over a full year in Marseille. Atmos. Chem. Phys. 17, 8247–8268.

Bozzetti, C., Sosedova, Y., Xiao, M., Daellenbach, K.R., Ulevicius, V., Dudoitis, V., Mordas, G., Byčenkienė, S., Plauškaitė, K., Vlachou, A., Golly, B., Chazeau, B., Besombes, J.L., Baltensperger, U., Jaffrezo, J.L., Slowik, J.G., El Haddad, I., Prévôt, A.S.H., 2017b. Argon offline-AMS source apportionment of organic aerosol over yearly cycles for an urban, rural, and marine site in northern Europe. Atmos. Chem. Phys. 17, 117–141.

Bruns, E.A., El Haddad, I., Slowik, J.G., Kilic, D., Klein, F., Baltensperger, U., Prévôt, A.S. H., 2016. Identification of significant precursor gases of secondary organic aerosols from residential wood combustion. Sci. Rep. 6, 27881.

Burnett, R., Chen, H., Szyszkowicz, M., Fann, N., Hubbell, B., Pope, C.A., Apte, J.S., Brauer, M., Cohen, A., Weichenthal, S., Coggins, J., Di, Q., Brunekreef, B., Frostad, J., Lim, S.S., Kan, H., Walker, K.D., Thurston, G.D., Hayes, R.B., Lim, C.C., Turner, M.C., Jerrett, M., Krewski, D., Gapstur, S.M., Diver, W.R., Ostro, B., Goldberg, D., Crouse, D.L., Martin, R.V., Peters, P., Pinault, L., Tjepkema, M., van Donkelaar, A., Villeneuve, P.J., Miller, A.B., Yin, P., Zhou, M., Wang, L., Janssen, N. A.H., Marra, M., Atkinson, R.W., Tsang, H., Thuan Quoc, T., Cannon, J.B., Allen, R. T., Hart, J.E., Laden, F., Cesaroni, G., Forastiere, F., Weinmayr, G., Jaensch, A., Nagel, G., Concin, H., Spadaro, J.V., 2018. Global estimates of mortality associated with long-term exposure to outdoor fine particulate matter. Proc. Natl. Acad. Sci. Unit. States Am. 115, 9592–9597.

Calvert, J.G., Derwent, R.G., Orlando, J.J., al, e., 2008. Mechanics of Atmospheric Oxidation of the Alkanes. Oxford University Press, Inc.

Canagaratna, M., Jayne, J., Jimenez, J., Allan, J., Alfarra, M., Zhang, Q., Onasch, T., Drewnick, F., Coe, H., Middlebrook, A., 2007. Chemical and microphysical characterization of ambient aerosols with the aerodyne aerosol mass spectrometer. Mass Spectrom. Rev. 26, 185–222.

Čanković, M., Zučko, J., Petrić, I., Margus, M., Ciglenečki, I., 2020. Impact of euxinic holomictic conditions on prokaryotic assemblages in a marine meromictic lake. Aquat. Microb. Ecol. 84, 141–154.

Canonaco, F., Crippa, M., Slowik, J., Baltensperger, U., Prévôt, A.S.H., 2013. SoFi, an IGOR-based interface for the efficient use of the generalized multilinear engine (ME-2) for the source apportionment: ME-2 application to aerosol mass spectrometer data. Atmos. Meas. Tech. 6, 3649–3661.

Canonaco, F., Tobler, A., Chen, G., Sosedova, Y., Slowik, J.G., Bozzetti, C., Daellenbach, K.R., El Haddad, I., Crippa, M., Huang, R.J., Furger, M., Baltensperger, U., Prévôt, A.S.H., 2021. A new method for long-term source apportionment with time-dependent factor profiles and uncertainty assessment using SoFi Pro: application to 1 year of organic aerosol data. Atmos. Meas. Tech. 14, 923–943.

Chen, Q., Farmer, D.K., Rizzo, L.V., Pauliquevis, T., Kuwata, M., Karl, T.G., Guenther, A., Allan, J.D., Coe, H., Andreae, M.O., Pöschl, U., Jimenez, J.L., Artaxo, P., Martin, S.T.,

2015. Submicron particle mass concentrations and sources in the Amazonian wet season (AMAZE-08). Atmos. Chem. Phys. 15, 3687–3701.
Chenoweth, J., Hadjinicolaou, P., Bruggeman, A., Lelieveld, J., Levin, Z., Lange, M.A., Xoplaki, E., Hadjikakou, M., 2011. Impact of climate change on the water resources of the eastern Mediterranean and Middle East region: modeled 21st century changes and implications. Water Resour. Res. 47, W06506.
Claeys, M., Graham, B., Vas, G., Wang, W., Vermeylen, R., Pashynska, V., Cafmeyer, J., Guyon, P., Andreae, M.O., Artaxo, P., Maenhaut, W., 2004. Formation of secondary organic aerosols through photooxidation of isoprene. Science 303, 1173–1176.
Claeys, M., Szmigielski, R., Vermeylen, R., Wang, W., Shalamzari, M.S., Maenhaut, W., 2013. Tracers for biogenic secondary organic aerosol from α-pinene and related monoterpenes: an overview. In: Barnes, I., Rudziński, K.J. (Eds.), Disposal of Dangerous Chemicals in Urban Areas and Mega Cities. Springer Netherlands, Dordrecht, pp. 227–238.
Crippa, M., Canonaco, F., Lanz, V.A., Äijälä, M., Allan, J.D., Carbone, S., Capes, G., Ceburnis, D., Dall'Osto, M., Day, D.A., DeCarlo, P.F., Ehn, M., Eriksson, A., Freney, E., Hildebrandt Ruiz, L., Hillamo, R., Jimenez, J.L., Junninen, H., Kiendler-Scharr, A., Kortelainen, A.M., Kulmala, M., Laaksonen, A., Mensah, A.A., Mohr, C., Nemitz, E., O'Dowd, C., Ovadnevaite, J., Pandis, S.N., Petäjä, T., Poulain, L., Saarikoski, S., Sellegri, K., Swietlicki, E., Tiitta, P., Worsnop, D.R., Baltensperger, U., Prévôt, A.S.H., 2014. Organic aerosol components derived from 25 AMS data sets across Europe using a consistent ME-2 based source apportionment approach. Atmos. Chem. Phys. 14, 6159–6176.
Crippa, M., El Haddad, I., Slowik, J.G., DeCarlo, P.F., Mohr, C., Heringa, M.F., Chirico, R., Marchand, N., Sciare, J., Baltensperger, U., Prévôt, A.S.H., 2013. Identification of marine and continental aerosol sources in Paris using high resolution aerosol mass spectrometry. J. Geophys. Res. Atmos. 118, 1950–1963.
Crosier, J., Allan, J.D., Coe, H., Bower, K.N., Formenti, P., Williams, P.I., 2007. Chemical composition of summertime aerosol in the Po valley (Italy), northern adriatic and black sea. Q. J. R. Meteorol. Soc. 133 (S1), 61–75.
Cvitešić Kušan, A., Frka, S., Ciglenečki, I., 2019. Electrochemical evidence of non-volatile reduced sulfur species in water-soluble fraction of fine marine aerosols. Atmosphere 10, 674.
Cvitešić Kušan, A., Kroflič, A., Grgić, I., Ciglenečki, I., Frka, S., 2020. Chemical characterization of fine aerosols in respect to water-soluble ions at the eastern Middle Adriatic coast. Environ. Sci. Pollut. Control Ser. 27, 10249–10264.
Daellenbach, K.R., Bozzetti, C., Křepelová, A., Canonaco, F., Wolf, R., Zotter, P., Fermo, P., Crippa, M., Slowik, J., Sosedova, Y., Zhang, Y., Huang, R.-J., Poulain, L., Szidat, S., Baltensperger, U., El Haddad, I., Prévôt, A.S.H., 2016. Characterization and source apportionment of organic aerosol using offline aerosol mass spectrometry. Atmos. Meas. Tech. 9, 23–39.
Daellenbach, K.R., El-Haddad, I., Karvonen, L., Vlachou, A., Corbin, J.C., Slowik, J.G., Heringa, M.F., Bruns, E.A., Luedin, S.M., Jaffrezo, J.-L., Szidat, S., Piazzalunga, A., Gonzalez, R., Fermo, P., Pflueger, V., Vogel, G., Baltensperger, U., Prévôt, A.S.H., 2018. Insights into organic-aerosol sources via a novel laser-desorption/ionization mass spectrometry technique applied to one year of PM10 samples from nine sites in central Europe. Atmos. Chem. Phys. 18, 2155–2174.
Daellenbach, K.R., Kourtchev, I., Vogel, A.L., Bruns, E.A., Jiang, J., Petäjä, T., Jaffrezo, J.-L., Aksoyoglu, S., Kalberer, M., Baltensperger, U., El Haddad, I., Prévôt, A.S.H., 2019. Impact of anthropogenic and biogenic sources on the seasonal variation of the molecular composition of urban organic aerosols: a field and laboratory study using ultra-high resolution mass spectrometry. Atmos. Chem. Phys. 19, 5973–5991.
Daellenbach, K.R., Stefenelli, G., Bozzetti, C., Vlachou, A., Fermo, P., Gonzalez, R., Piazzalunga, A., Colombi, C., Canonaco, F., Hueglin, C., Kasper-Giebl, A., Jaffrezo, J.-L., Bianchi, F., Slowik, J.G., Baltensperger, U., El Haddad, I., Prévôt, A.S.H., 2017. Long-term chemical analysis and organic aerosol source apportionment at nine sites in central Europe: source identification and uncertainty assessment. Atmos. Chem. Phys. 17, 13265–13282.
Daellenbach, K.R., Uzu, G., Jiang, J., Cassagnes, L.-E., Leni, Z., Vlachou, A., Stefenelli, G., Canonaco, F., Weber, S., Segers, A., 2020. Sources of particulate-matter air pollution and its oxidative potential in Europe. Nature 587, 414–419.
De Pieri, S., Arruti, A., Huremovic, J., Sulejmanovic, J., Selovic, A., Đorđević, D., Fernández-Olmo, I., Gambaro, A., 2014. PAHs in the urban air of Sarajevo: levels, sources, day/night variation, and human inhalation risk. Environ. Monit. Assess. 186, 1409–1419.
DeCarlo, P.F., Kimmel, J.R., Trimborn, A., Northway, M.J., Jayne, J.T., Aiken, A.C., Gonin, M., Fuhrer, K., Horvath, T., Docherty, K.S., Worsnop, D.R., Jimenez, J.L., 2006. Field-Deployable, high-resolution, time-of-flight aerosol mass spectrometer. Anal. Chem. 78, 8281–8289.
Dockery, D.W., Pope, C.A., Xu, X., Spengler, J.D., Ware, J.H., Fay, M.E., Ferris, B.G., Speizer, F.E., 1993. An association between air pollution and mortality in six U.S. Cities. N. Engl. J. Med. 329, 1753–1759.
Dockery, D.W., Schwartz, J., Spengler, J.D., 1992. Air pollution and daily mortality: associations with particulates and acid aerosols. Environ. Res. 59, 362–373.
Duplissy, J., DeCarlo, P.F., Dommen, J., Alfarra, M.R., Metzger, A., Barmpadimos, I., Prevot, A.S.H., Weingartner, E., Tritscher, T., Gysel, M., Aiken, A.C., Jimenez, J.L., Canagaratna, M.R., Worsnop, D.R., Collins, D.R., Tomlinson, J., Baltensperger, U., 2011. Relating hygroscopicity and composition of organic aerosol particulate matter. Atmos. Chem. Phys. 11, 1155–1165.
García-Ruiz, J.M., López-Moreno, J.I., Vicente-Serrano, S.M., Lasanta–Martínez, T., Beguería, S., 2011. Mediterranean water resources in a global change scenario. Earth Sci. Rev. 105, 121–139.
Giorgi, F., Lionello, P., 2008. Climate change projections for the Mediterranean region. Global Planet. Change 63, 90–104.
Gregoris, E., Morabito, E., Barbaro, E., Feltracco, M., Toscano, G., Merico, E., Grasso, F. M., Cesari, D., Conte, M., Contini, D., Gambaro, A., 2021. Chemical characterization and source apportionment of size-segregated aerosol in the port-city of Venice (Italy). Atmos. Pollut. Res. 12, 261–271.
Guenther, A., Hewitt, C.N., Erickson, D., Fall, R., Geron, C., Graedel, T., Harley, P., Klinger, L., Lerdau, M., McKay, W.A., Pierce, T., Scholes, B., Steinbrecher, R., Tallamraju, R., Taylor, J., Zimmerman, P., 1995. A global model of natural volatile organic compound emissions. J. Geophys. Res. Atmos. 100, 8873–8892.
Highwood, E.J., Haywood, J.M., Coe, H., Cook, J., Osborne, S., Williams, P., Crosier, J., Bower, K., Formenti, P., McQuaid, J., Brooks, B., Thomas, G., Grainger, R., Barnaba, F., Gobbi, G.P., de Leeuw, G., Hopkins, J., 2007. Aerosol direct radiative impact experiment (ADRIEX) overview. Q. J. R. Meteorol. Soc. 133, 3–15.
Hildebrandt, L., Engelhart, G.J., Mohr, C., Kostenidou, E., Lanz, V.A., Bougiatioti, A., DeCarlo, P.F., Prevot, A.S.H., Baltensperger, U., Mihalopoulos, N., Donahue, N.M., Pandis, S.N., 2010. Aged organic aerosol in the eastern mediterranean: the finokalia aerosol measurement experiment – 2008. Atmos. Chem. Phys. 10, 4167–4186.
Huremović, J., Žero, S., Bubalo, E., Dacić, M., Čeliković, A., Musić, I., Bašić, M., Huseinbašić, N., Džepina, K., Cepić, M., Muratović, N., Pašalić, A., Salihagić, S., Krvavac, Z., Zelić-Hadžiomerović, J., Gojak-Salimović, S., 2020. Analysis of PM10, Pb, Cd, and Ni atmospheric concentrations during domestic heating season in Sarajevo, Bosnia and Herzegovina, from 2010 to 2019. Air Qual. Atmos. Health 13, 965–976.
IPCC, 2021. Climate Change 2021: the Physical Science Basis. Contribution of Working Group I to the Sixth Assessment Report of the Intergovernmental Panel on Climate Change. IPCC, Geneva, Switzerland.
Jaeckels, J.M., Bae, M.-S., Schauer, J.J., 2007. Positive matrix factorization (PMF) analysis of molecular marker measurements to quantify the sources of organic aerosols. Environ. Sci. Technol. 41, 5763–5769.
Jimenez, J.L., Canagaratna, M.R., Donahue, N.M., Prevot, A.S.H., Zhang, Q., Kroll, J.H., DeCarlo, P.F., Allan, J.D., Coe, H., Ng, N.L., Aiken, A.C., Docherty, K.S., Ulbrich, I. M., Grieshop, A.P., Robinson, A.L., Duplissy, J., Smith, J.D., Wilson, K.R., Lanz, V.A., Hueglin, C., Sun, Y.L., Tian, J., Laaksonen, A., Raatikainen, T., Rautiainen, J., Vaattovaara, P., Ehn, M., Kulmala, M., Tomlinson, J.M., Collins, D.R., Cubison, M.J., null, n., Dunlea, J., Huffman, J.A., Onasch, T.B., Alfarra, M.R., Williams, P.I., Bower, K., Kondo, Y., Schneider, J., Drewnick, F., Borrmann, S., Weimer, S., Demerjian, K., Salcedo, D., Cottrell, L., Griffin, R., Takami, A., Miyoshi, T., Hatakeyama, S., Shimono, A., Sun, J.Y., Zhang, Y.M., Dzepina, K., Kimmel, J.R., Sueper, D., Jayne, J.T., Herndon, S.C., Trimborn, A.M., Williams, L.R., Wood, E.C., Middlebrook, A.M., Kolb, C.E., Baltensperger, U., Worsnop, D.R., 2009. Evolution of organic aerosols in the atmosphere. Science 326, 1525–1529.
Kanakidou, M., Mihalopoulos, N., Kindap, T., Im, U., Vrekoussis, M., Gerasopoulos, E., Dermitzaki, E., Unal, A., Koçak, M., Markakis, K., Melas, D., Kouvarakis, G., Youssef, A.F., Richter, A., Hatzianastassiou, N., Hilboll, A., Ebojie, F., Wittrock, F., von Savigny, C., Burrows, J.P., Ladstaetter-Weissenmayer, A., Moubasher, H., 2011. Megacities as hot spots of air pollution in the East Mediterranean. Atmos. Environ. 45, 1223–1235.
Kodros, J.K., Papanastasiou, D.K., Paglione, M., Masiol, M., Squizzato, S., Florou, K., Skyllakou, K., Kaltsonoudis, C., Nenes, A., Pandis, S.N., 2020. Rapid dark aging of biomass burning as an overlooked source of oxidized organic aerosol. Proc. Natl. Acad. Sci. Unit. States Am. 117, 33028.
Kostenidou, E., Florou, K., Kaltsonoudis, C., Tsiflikiotou, M., Vratolis, S., Eleftheriadis, K., Pandis, S.N., 2015. Sources and chemical characterization of organic aerosol during the summer in the eastern Mediterranean. Atmos. Chem. Phys. 15, 11355–11371.
Kostenidou, E., Kaltsonoudis, C., Tsiflikiotou, M., Louvaris, E., Russell, L.M., Pandis, S.N., 2013. Burning of olive tree branches: a major organic aerosol source in the Mediterranean. Atmos. Chem. Phys. 13, 8797–8811.
Lanz, V., Alfarra, M., Baltensperger, U., Buchmann, B., Hueglin, C., Prévôt, A.S.H., 2007. Source apportionment of submicron organic aerosols at an urban site by factor analytical modelling of aerosol mass spectra. Atmos. Chem. Phys. 7, 1503–1522.
Leaitch, W.R., Macdonald, A.M., Brickell, P.C., Liggio, J., Sjostedt, S.J., Vlasenko, A., Bottenheim, J.W., Huang, L., Li, S.-M., Liu, P.S.K., Toom-Sauntry, D., Hayden, K.A., Sharma, S., Shantz, N.C., Wiebe, H.A., Zhang, W., Abbatt, J.P.D., Slowik, J.G., Chang, R.Y.W., Russell, L.M., Schwartz, R.E., Takahama, S., Jayne, J.T., Ng, N.L., 2011. Temperature response of the submicron organic aerosol from temperate forests. Atmos. Environ. 45, 6696–6704.
Lelieveld, J., Berresheim, H., Borrmann, S., Crutzen, P.J., Dentener, F.J., Fischer, H., Feichter, J., Flatau, P.J., Heland, J., Holzinger, R., Korrmann, R., Lawrence, M.G., Levin, Z., Markowicz, K.M., Mihalopoulos, N., Minikin, A., Ramanathan, V., Reus, M. d., Roelofs, G.J., Scheeren, H.A., Sciare, J., Schlager, H., Schultz, M., Siegmund, P., Steil, B., Stephanou, E.G., Stier, P., Traub, M., Warneke, C., Williams, J., Ziereis, H., 2002. Global air pollution crossroads over the mediterranean. Science 298, 794–799.
Lelieveld, J., Hadjinicolaou, P., Kostopoulou, E., Chenoweth, J., El Maayar, M., Giannakopoulos, C., Hannides, C., Lange, M.A., Tanarhte, M., Tyrlis, E., Xoplaki, E., 2012. Climate change and impacts in the eastern mediterranean and the Middle East. Climatic Change 114, 667–687.
Lopez-Hilfiker, F.D., Pospisilova, V., Huang, W., Kalberer, M., Mohr, C., Stefenelli, G., Thornton, J.A., Baltensperger, U., Prevot, A.S.H., Slowik, J.G., 2019. An extractive electrospray ionization time-of-flight mass spectrometer (EESI-TOF) for online measurement of atmospheric aerosol particles. Atmos. Meas. Tech. 12, 4867–4886.
Merico, E., Donateo, A., Gambaro, A., Cesari, D., Gregoris, E., Barbaro, E., Dinoi, A., Giovanelli, G., Masieri, S., Contini, D., 2016. Influence of in-port ships emissions to gaseous atmospheric pollutants and to particulate matter of different sizes in a Mediterranean harbour in Italy. Atmos. Environ. 139, 1–10.
Mifka, B., Žurga, P., Kontošić, D., Odorčić, D., Mezlar, M., Merico, E., Grasso, F.M., Conte, M., Contini, D., Alebić-Juretić, A., 2021. Characterization of airborne

particulate fractions from the port city of Rijeka, Croatia. Mar. Pollut. Bull. 166, 112236.
Millero, F.J., 2013. Chemical Oceanography, fourth ed. ed. CRC Press.
Mohr, C., DeCarlo, P.F., Heringa, M.F., Chirico, R., Richter, R., Crippa, M., Querol, X., Baltensperger, U., Prévôt, A.S.H., 2015. Spatial variation of aerosol chemical composition and organic components identified by positive matrix factorization in the barcelona region. Environ. Sci. Technol. 49, 10421–10430.
Mutzel, A., Rodigast, M., Iinuma, Y., Böge, O., Herrmann, H., 2016. Monoterpene SOA – contribution of first-generation oxidation products to formation and chemical composition. Atmos. Environ. 130, 136–144.
ORNL, D., 2017. Spatial Data Access Tool (SDAT). ORNL DAAC. Oak Ridge, Tennessee, USA. (Accessed 10 June 2021).
Paatero, P., 1999. The multilinear engine—a table-driven, least squares program for solving multilinear problems, including the n-way parallel factor analysis model. J. Comput. Graph Stat. 8, 854–888.
Pehnec, G., Jakovljević, I., Godec, R., Sever Štrukil, Z., Žero, S., Huremović, J., Džepina, K., 2020. Carcinogenic organic content of particulate matter at urban locations with different pollution sources. Sci. Total Environ. 734, 139414.
Pieber, S.M., El Haddad, I., Slowik, J.G., Canagaratna, M.R., Jayne, J.T., Platt, S.M., Bozzetti, C., Daellenbach, K.R., Fröhlich, R., Vlachou, A., Klein, F., Dommen, J., Miljevic, B., Jiménez, J.L., Worsnop, D.R., Baltensperger, U., Prévôt, A.S.H., 2016. Inorganic salt interference on CO_2^+ in aerodyne AMS and ACSM organic aerosol composition studies. Environ. Sci. Technol. 50, 10494–10503.
Platt, S.M., Haddad, I.E., Pieber, S.M., Huang, R.J., Zardini, A.A., Clairotte, M., Suarez-Bertoa, R., Barmet, P., Pfaffenberger, L., Wolf, R., Slowik, J.G., Fuller, S.J., Kalberer, M., Chirico, R., Dommen, J., Astorga, C., Zimmermann, R., Marchand, N., Hellebust, S., Temime-Roussel, B., Baltensperger, U., Prévôt, A.S.H., 2014. Two-stroke scooters are a dominant source of air pollution in many cities. Nat. Commun. 5, 3749.
Qi, L., Chen, M., Stefenelli, G., Pospisilova, V., Tong, Y., Bertrand, A., Hueglin, C., Ge, X., Baltensperger, U., Prévôt, A.S.H., Slowik, J.G., 2019. Organic aerosol source apportionment in Zurich using an extractive electrospray ionization time-of-flight mass spectrometer (EESI-TOF-MS) – Part 2: biomass burning influences in winter. Atmos. Chem. Phys. 19, 8037–8062.
Qi, L., Vogel, A.L., Esmaeilirad, S., Cao, L., Zheng, J., Jaffrezo, J.L., Fermo, P., Kasper-Giebl, A., Daellenbach, K.R., Chen, M., Ge, X., Baltensperger, U., Prévôt, A.S.H., Slowik, J.G., 2020. A 1-year characterization of organic aerosol composition and sources using an extractive electrospray ionization time-of-flight mass spectrometer (EESI-TOF). Atmos. Chem. Phys. 20, 7875–7893.
Sanchez-Gomez, E., Somot, S., Mariotti, A., 2009. Future changes in the Mediterranean water budget projected by an ensemble of regional climate models. Geophys. Res. Lett. 36.
Schneider, J., Weimer, S., Drewnick, F., Borrmann, S., Helas, G., Gwaze, P., Schmid, O., Andreae, M.O., Kirchner, U., 2006. Mass spectrometric analysis and aerodynamic properties of various types of combustion-related aerosol particles. Int. J. Mass Spectrom. 258, 37–49.
Škarek, M., Ćupr, P., Bartoš, T., Kohoutek, J., Klánová, J., Holoubek, I., 2007. A combined approach to the evaluation of organic air pollution —a case study of urban air in Sarajevo and Tuzla(Bosnia and Herzegovina). Sci. Total Environ. 384, 182–193.
Srivastava, D., Daellenbach, K.R., Zhang, Y., Bonnaire, N., Chazeau, B., Perraudin, E., Gros, V., Lucarelli, F., Villenave, E., Prévôt, A.S.H., El Haddad, I., Favez, O., Albinet, A., 2021. Comparison of five methodologies to apportion organic aerosol sources during a PM pollution event. Sci. Total Environ. 757, 143168.
Stanic, N., Kraljević, T., Talić, S., 2012. Variation of PM10, NO2, NO and O3 in city of mostar, Bosnia and Herzegovina. Bulletin of the Chemists and Technologists of Bosnia and Herzegovina 7–10.
Stefenelli, G., Pospisilova, V., Lopez-Hilfiker, F.D., Daellenbach, K.R., Hüglin, C., Tong, Y., Baltensperger, U., Prévôt, A.S.H., Slowik, J.G., 2019. Organic aerosol source apportionment in Zurich using an extractive electrospray ionization time-of-flight mass spectrometer (EESI-TOF-MS)–Part 1: biogenic influences and day–night chemistry in summer. Atmos. Chem. Phys. 19, 14825–14848.
Talić, S., Martinović Bevanda, A., Ćurlin, M., Kraljević, T., 2018. Seasonal variations of NO2, O3, and PM10 in mostar, Bosnia and Herzegovina. In: Physical Chemistry 2018 14th International Conference on Fundamental and Applied Aspects of Physical Chemistry, Belgrade, Serbia, pp. 781–784.
Tong, Y., Pospisilova, V., Qi, L., Duan, J., Gu, Y., Kumar, V., Rai, P., Stefenelli, G., Wang, L., Wang, Y., Zhong, H., Baltensperger, U., Cao, J., Huang, R.J., Prévôt, A.S.H., Slowik, J.G., 2021. Quantification of solid fuel combustion and aqueous chemistry contributions to secondary organic aerosol during wintertime haze events in Beijing. Atmos. Chem. Phys. 21, 9859–9886.
Turšič, J., Podkrajšek, B., Grgić, I., Ctyroky, P., Berner, A., Dusek, U., Hitzenberger, R., 2006. Chemical composition and hygroscopic properties of size-segregated aerosol particles collected at the Adriatic coast of Slovenia. Chemosphere 63, 1193–1202.
Vlachou, A., Daellenbach, K.R., Bozzetti, C., Chazeau, B., Salazar, G.A., Szidat, S., Jaffrezo, J.L., Hueglin, C., Baltensperger, U., Haddad, I.E., Prévôt, A.S.H., 2018. Advanced source apportionment of carbonaceous aerosols by coupling offline AMS and radiocarbon size-segregated measurements over a nearly 2-year period. Atmos. Chem. Phys. 18, 6187–6206.
Vlachou, A., Tobler, A., Lamkaddam, H., Canonaco, F., Daellenbach, K.R., Jaffrezo, J.L., Minguillón, M.C., Maasikmets, M., Teinemaa, E., Baltensperger, U., El Haddad, I., Prévôt, A.S.H., 2019. Development of a versatile source apportionment analysis based on positive matrix factorization: a case study of the seasonal variation of organic aerosol sources in Estonia. Atmos. Chem. Phys. 19, 7279–7295.
Wang, D.S., Lee, C.P., Krechmer, J.E., Majluf, F., Tong, Y., Canagaratna, M.R., Schmale, J., Prévôt, A.S.H., Baltensperger, U., Dommen, J., El Haddad, I., Slowik, J. G., Bell, D.M., 2021. Constraining the response factors of an extractive electrospray ionization mass spectrometer for near-molecular aerosol speciation. Atmos. Meas. Tech. Discuss. 14, 6955–6972. https://doi.org/10.5194/amt-14-6955-2021.
WHO, 2018. World Health Organization Mortality Database last updated on 11th April.
Xu, L., Guo, H., Boyd, C.M., Klein, M., Bougiatioti, A., Cerully, K.M., Hite, J.R., Isaacman-VanWertz, G., Kreisberg, N.M., Knote, C., Olson, K., Koss, A., Goldstein, A.H., Hering, S.V., de Gouw, J., Baumann, K., Lee, S.-H., Nenes, A., Weber, R.J., Ng, N.L., 2015. Effects of anthropogenic emissions on aerosol formation from isoprene and monoterpenes in the southeastern United States. Proc. Natl. Acad. Sci. Unit. States Am. 112 (1), 37–42. https://doi.org/10.1073/pnas.1417609112.
Ye, J., Abbatt, J.P.D., Chan, A.W.H., 2018. Novel pathway of SO2 oxidation in the atmosphere: reactions with monoterpene ozonolysis intermediates and secondary organic aerosol. Atmos. Chem. Phys. 18, 5549–5565.
Zhou, S., Collier, S., Jaffe, D.A., Briggs, N.L., Hee, J., Sedlacek Iii, A.J., Kleinman, L., Onasch, T.B., Zhang, Q., 2017. Regional influence of wildfires on aerosol chemistry in the western US and insights into atmospheric aging of biomass burning organic aerosol. Atmos. Chem. Phys. 17, 2477–2493.